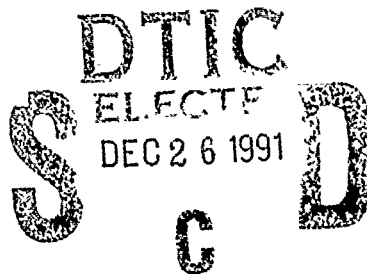


AD-A243 965



AFIT/ENS/GSO/91D-04



A Top-Down Performance Analysis
of a
Pegasus-Based Space Strike System

THESIS

Douglas Emil Collins
Captain, USAF

AFIT/ENS/GSO/91D-04

Approved for public release; distribution unlimited

91-19019



91 12 24 039

REPORT DOCUMENTATION PAGE			Form Approved OMB No. 0704-0188	
Public reporting burden for this collection of information is estimated to average 1 hour per response, including the time for reviewing instructions, searching existing data sources, gathering and maintaining the data needed, and completing and reviewing the collection of information. Send comments regarding this burden estimate or any other aspect of this collection of information, including suggestions for reducing this burden, to Washington Headquarters Services, Directorate for Information Operations and Reports, 1215 Jefferson Davis Highway, Suite 1204, Arlington, VA 22202-4302, and to the Office of Management and Budget, Paperwork Reduction Project (0704-0188), Washington, DC 20503.				
1. AGENCY USE ONLY (Leave blank)		2. REPORT DATE December 1991		3. REPORT TYPE AND DATES COVERED Master's Thesis
4. TITLE AND SUBTITLE A TOP-DOWN PERFORMANCE ANALYSIS OF A PEGASUS-BASED SPACE STRIKE SYSTEM			5. FUNDING NUMBERS	
6. AUTHOR(S) Douglas E. Collins, Captain, USAF				
7. PERFORMING ORGANIZATION NAME(S) AND ADDRESS(ES) Air Force Institute of Technology, WPAFB OH 45433-6583			8. PERFORMING ORGANIZATION REPORT NUMBER AFIT/GSO/ENS/91D-04	
9. SPONSORING/MONITORING AGENCY NAME(S) AND ADDRESS(ES) AFSPACECOM/XPDF Peterson AFB CO 80914			10. SPONSORING/MONITORING AGENCY REPORT NUMBER	
11. SUPPLEMENTARY NOTES				
12a. DISTRIBUTION/AVAILABILITY STATEMENT Approved for public release; distribution unlimited			12b. DISTRIBUTION CODE	
13. ABSTRACT (Maximum 200 words) <p>The feasibility of using the Pegasus launch vehicle as a conventional weapons platform is examined. Using a top-down approach, the analysis addresses the fundamental question of whether such a system should be considered for development. The measures of effectiveness considered are delivery range, probability of destroying the target, and responsiveness. Each of the measures is assessed at its top-level and analyzed only to the level of detail needed to address the fundamental question. The study indicates that attaining a high probability of destroying the target requires extremely precise control over the burnout conditions and that the system must be on constant ready standby to achieve short response times.</p>				
14. SUBJECT TERMS Pegasus, Space to Ground, Space Warfare			15. NUMBER OF PAGES 98	
			16. PRICE CODE	
17. SECURITY CLASSIFICATION OF REPORT Unclassified	18. SECURITY CLASSIFICATION OF THIS PAGE Unclassified	19. SECURITY CLASSIFICATION OF ABSTRACT Unclassified	20. LIMITATION OF ABSTRACT UL	

A Top-Down Performance Analysis
of a
Pegasus-Based Space Strike System

THESIS

Presented to the Faculty of the School of Engineering
of the Air Force Institute of Technology
Air University

In Partial Fulfillment of the
Requirements for the Degree of
Master of Science (Space Operations)

Douglas Emil Collins, B.S.
Captain, USAF

December, 1991



Accession For	
NTIS GRA&I	<input checked="checked" type="checkbox"/>
DTIC TAB	<input type="checkbox"/>
Unannounced	<input type="checkbox"/>
Justification	
By	
Distribution/	
Availability Codes	
Dist	Avail and/or Special
A-1	

Thesis Approval

Student: Captain Douglas E. Collins

Section: GSO 91D

Thesis Title: A Top-Down Performance Analysis of a Pegasus-Based Space Strike System

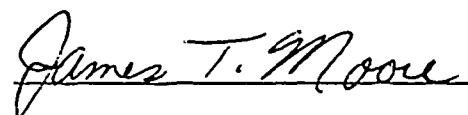
Defense Date: November 27, 1991

COMMITTEE	NAME/DEPARTMENT	SIGNATURE
-----------	-----------------	-----------

Advisor	Major Paul F. Auclair/ENS	
---------	---------------------------	--



Reader	Lieutenant Colonel James T. Moore/ENS	
--------	---------------------------------------	--



Acknowledgments

This work is dedicated to my daughter, Amanda, with the hope that her accomplishments will one day eclipse mine. I thank God for giving me silent encouragement to keep up, and my advisor, Major Paul Auclair, for being the only AFIT instructor to present an *approach* to analysis as opposed to an analytical *tool*—and for beating it into my head until I understood.

Douglas Emil Collins

Table of Contents

	Page
Acknowledgments	ii
Table of Contents	iii
List of Figures	vi
List of Tables	viii
Abstract	ix
 I. Introduction	 1
1.1 Categories of Force Application Weapons	2
1.2 Overview of Current Developments	2
1.3 Statement of the Problem	3
1.4 Purpose of the Study	3
1.5 Definition of Measures of Effectiveness	3
1.6 Operational Assumptions	4
1.7 Subsequent Chapters	5
 II. Background on Space Strike Weapons and the Pegasus Space Launch Vehicle	 6
2.1 Perspectives on Space Strike Weapons	6
2.1.1 History	6
2.1.2 International Law and Agreements	7
2.1.3 Concurrence with Air Force Strategy	8
2.2 The Pegasus Space Launch System	9
2.2.1 Overview	9

	Page
2.2.2 System Description	9
2.2.3 Pegasus Mission Profile	10
2.2.4 Adaptations for Space Strike Missions	11
2.3 Chapter Summary	12
III. Research Method and Analysis Foundations	13
3.1 Top-Down Analysis	13
3.2 Fundamentals of Space Flight Analysis	18
3.2.1 Introduction	18
3.2.2 Basic Relationships	21
3.2.3 Ballistic Trajectory Analysis	25
3.3 Solid Rocket Terms and Relations	36
3.4 Chapter Summary	36
IV. Top-Down Performance Analysis	38
4.1 Overview	38
4.1.1 Trajectory Range	38
4.1.2 Probability of Target Destruction	38
4.1.3 Pegasus Responsiveness	39
4.2 Range Axis Analysis	41
4.3 Target Destruction Axis Analysis	42
4.3.1 CEP Determination	43
4.4 Responsiveness Axis Analysis	51
4.4.1 Mission phases	52
4.4.2 USAF B-52 operations	53
4.4.3 Readiness Assessment	57
4.4.4 Responsiveness and Reliability	57
4.5 "Backing In": a GPRC Example	57

	Page
4.5.1 GPRC Responsiveness	57
4.5.2 GPRC Precision	58
4.6 Chapter Summary	60
V. Conclusions	61
Appendix A. Pegasus Performance Boundaries	63
Appendix B. Burnout Parameter Interactions	66
B.1 Re-entry Location Displacement	66
B.1.1 Down-range Displacement	67
B.1.2 Cross-range Displacement	75
B.2 Influence Coefficient Determination	75
Appendix C. Ancillary Effects	78
C.1 Earth Oblateness Effects	78
C.2 Atmospheric Drag During Re-entry	80
C.3 Rotating Earth Effects	82
C.3.1 Terms and Reference Frames	82
C.3.2 Burnout Conditions	82
C.3.3 Re-entry Location Determination	84
Bibliography	86
Vita	88

List of Figures

Figure	Page
1. Pegasus Cutaway Drawing (reproduced from (5:5.33))	10
2. Typical Pegasus Mission Profile (reproduced from (5:5.36))	11
3. Traditional Analysis Decision Space	14
4. Typical Top-Down Analysis Decision Space	16
5. Geocentric-Equatorial Coordinate System (reproduced from (1:55))	19
6. Orbital Elements (reproduced from (20:58))	20
7. Vehicle Dependent Parameters (reproduced from (1:17))	22
8. Ballistic Trajectory Phases (reproduced from (1:281))	26
9. Symmetry Effects (reproduced from (1:283))	28
10. Ellipse Geometry (reproduced from (1:287))	30
11. Cross-range Error Analysis (reproduced from (1:299))	35
12. Range Axis Analysis Levels	39
13. PD Axis Analysis Levels	40
14. Responsiveness Axis Analysis Levels	41
15. Parameter Requirements for Given Delivery Ranges	42
16. Q Value vs. Velocity	43
17. Q Value vs. Burnout Altitude	44
18. Probability of Destruction: CEP vs. Target Radius	45
19. Maximum Down- and Cross-range Standard Deviation: Circular Dispersion	46
20. Maximum Down- and Cross-range Standard Deviation: Elliptic Dispersion	47
21. Bias Effects on CEP: Circular Dispersion	48
22. Bias-Limited Down- and Cross-range Displacement	50
23. Down-range Displacement Due to Burnout Velocity Error	51

Figure	Page
24. Down-range Displacement Due to Burnout Altitude Error	52
25. Cross-range Displacement Due to Burnout Azimuth Error	53
26. Cross-range Displacement Due to Lateral Burnout Point Displacement	54
27. Pegasus Motor Characteristics (reproduced from (13:2-5))	63
28. Pegasus Theoretical Velocity vs. Payload	64
29. Theoretical 2-stage Pegasus Maximum Burnout Altitude	65
30. Free-flight Range (Ψ) vs. Q -value	67
31. Free-flight Range (Ψ) vs. Flight-path Angle (ϕ)	68
32. Typical 2-stage Velocity Error Effects, High vs. Low Trajectories . .	69
33. Typical 2-stage Velocity Error Effects, Fixed Flight-path Angle . . .	70
34. Typical 3-stage Velocity Error Effects, Fixed Flight-path Angle . . .	71
35. Typical Altitude Error Effects, High vs. Low Trajectories	72
36. Typical 2-stage Altitude Error Effects, Fixed Flight-path Angle . . .	72
37. Typical 3-stage Altitude Error Effects, Fixed Flight-path Angle . . .	73
38. Selected Range-angle/Flight-path Angle Curves	74
39. Cross-range Errors Due to Burnout Azimuth Error	76
40. Cross-range Errors Due to Lateral Burnout Point Displacement . . .	77
41. Typical Ballistic Re-Entry Drag Effect (reproduced from (20:224)) .	81
42. Velocity Components in the TII System (reproduced from (1:309)) .	83
43. Velocity Effects of Earth Rotation	84

List of Tables

Table	Page
1. Eccentricity-Orbit Shape Relationship	21
2. Forces Acting on a Ballistic Trajectoried Vehicle	27
3. Parameter Error Influence Coefficients: Down-range Effects	49
4. Parameter Error Influence Coefficients: Cross-range Effects	49
5. Preflight Phase Time Bounds	56
6. Maximum Allowable Parameter Errors: 30 Meter Bias	59
7. Typical Pegasus Parameter Combinations	68
8. Typical 2-Stage Flight-path Angle (ϕ) Error Displacement Effects . .	74
9. Typical 3-stage Flight-path Angle (ϕ) Error Displacement Effects . .	75
10. Down-Range Displacement Influence Coefficients	76

Abstract

The feasibility of using the Pegasus launch vehicle as a conventional weapons platform is examined. Using a top-down approach, the analysis addresses the fundamental question of whether such a system should be considered for development. The measures of effectiveness considered are delivery range, probability of destroying the target, and responsiveness. Each of the measures is assessed at its top-level and analyzed only to the level of detail needed to address the fundamental question. The study indicates that attaining a high probability of destroying the target requires extremely precise control over the burnout conditions and that the system must be on constant ready standby to achieve short response times.

A Top-Down Performance Analysis of a Pegasus-Based Space Strike System

I. Introduction

The Reagan administration published its policy regarding Department of Defense (DoD) space activities in March, 1987. The "General Policy" section stated that "(s)pace is recognized as being a medium within which the conduct of military operations in support of our national security can take place . . . and from which the military space functions of space support, force enhancement, space control and *force application* can be performed" (9:2) (emphasis added). Force application received little further definition except that "force application functions consist of combat operations conducted from space" (9:5). The context of the surrounding text indicated that such operations referred primarily to efforts then underway in the area of ballistic missile defense and the Strategic Defense Initiative (SDI) (9:5).

The newly elected Bush administration published its own space policy in November, 1989. The DoD was assigned the same four space functions, but force application was no longer tied solely to missile defense. In fact, discussion of SDI had been moved to an entirely separate section titled "General Guidelines" (10:5).

Based on published U.S. space policy, the United States Air Force (USAF) is formalizing its role in space through the creation of a dedicated doctrine. The draft of this manual, titled *Space Operations*, describes mission areas corresponding to each of the four DoD space functions. Force application is defined therein as follows:

Force application includes combat operations conducted from space for the purpose of affecting terrestrial conflicts. It encompasses the Air Force basic missions of strategic aerospace defense, counter air, air interdiction, and close air support (21:38).

The draft manual implies the potential for USAF development and use of exoatmospheric systems to affect terrestrial conflict.

1.1 Categories of Force Application Weapons

The means of applying force from space can be grouped into two general categories—space based systems and space transient systems. Space based systems might take the form of armed orbiting vehicles designed to strike targets either in the atmosphere or on the ground. Space transient systems spend only a part of their mission lives in the medium of space and strike their targets by following a ballistic or suborbital trajectory. Examples of the latter exist currently in the form of nuclear-weapon armed intercontinental ballistic missile (ICBMs) and submarine launched ballistic missiles (SLBMs). Although such systems would probably not be used in a limited conflict, non-nuclear, ballistic trajectory weapons could provide the basis for near-term force application systems. The recent Persian Gulf war demonstrated the efficacy of highly accurate conventional weapons delivered to the target by combat aircraft. The difficulties encountered during the 1986 Libyan mission illustrated some of the drawbacks to this type of delivery: overflight restrictions, aircraft range limitations, and attrition due to hostile defenses. A highly accurate space transient weapon could provide an attractive means of hitting high value targets while avoiding these limitations.

1.2 Overview of Current Developments

Two American companies, Orbital Sciences Corporation (OSC) and Hercules Aerospace Company, began a privately funded program in 1987 to develop a new space launch system. It would be capable of placing small payloads into orbit cheaply and with great flexibility. The result of this effort is a space launch system consisting of a solid-rocket propelled booster dropped from high altitude by a carrier aircraft. Once released, the rocket is designed to ignite, climb through the atmosphere, and deliver its payload to orbit. The new system, designated 'Pegasus', successfully delivered its first two-satellite payload into low Earth orbit on April 5th, 1990 (11:1).

A weapons delivery system based on Pegasus could provide an effective means of fulfilling the force application mission. Air Force Space Command (AFSPACECOM) sponsored research into this concept has already resulted in at least one design called "Global Precision Response Capability (GPRC)", which uses the Pegasus vehicle as a means of delivery for a cluster of small kinetic energy (KE) warheads (16:4). Advocates of the system imbue it with "surgical precision" and "less than four hour

response time" (16:5). If such claims are valid, a GPRC-like system could provide a low-risk, highly effective addition to U.S. military capability.

1.3 Statement of the Problem

Planners at AFSPACECOM headquarters are interested in the potential of a Pegasus-derived strike system such as that given in GPRC. There is little material available that can be used to independently substantiate claims made by system proponents concerning potential strike capability, and funds for an exhaustive study are not available. An independent means of judging performance assertions is needed to better determine if the concept is worth pursuing.

1.4 Purpose of the Study

This thesis intends to provide AFSPACECOM personnel with an understanding of how a "top-down" approach to this type of problem can be used to establish performance requirements that must be achieved by a system like Pegasus before embarking on its development. The research intends to identify those factors that drive performance capabilities and to set reasonable bounds on expected Pegasus performance in a ballistic trajectoried strike role.

1.5 Definition of Measures of Effectiveness

This thesis uses three broad measures of effectiveness (MOEs) to evaluate the efficacy of the Pegasus-based system: probability of target destruction (PD), weapon range, and system responsiveness.

PD is a function of both weapon and target characteristics. The unclassified nature of this study precludes a detailed discussion of potential weapons, assuming only that warheads will be limited to conventional (i.e., non-nuclear) designs. Likewise, specific target types will not be examined except with regard to general characteristics (relative sizes, hardness, etc.). PD will therefore be evaluated as a function of Pegasus delivery accuracy and relative target characteristics.

The accuracy of a ballistic weapon system describes its ability to deliver one or more warheads to a specified target location. "Perfect" accuracy would guarantee a precise delivery but, in reality, most weapons "miss" their intended aim points by some distance. The distribution of these miss distances characterizes the accuracy of

a particular weapon system. A common measure of a weapon's accuracy is "circular error probable (CEP)", defined as "the radius of a circle centered at the target or mean point of impact within which the probability of impact is 0.5 " (2:1-1). CEP values do not indicate that a given warhead will certainly fall within the distance given, but rather that on average, *fifty-percent* of the warheads fired at a given location will fall within the CEP distance. It is equally likely, then, for a given warhead to fall either inside or outside the listed CEP. The effect of a 100 kiloton nuclear airburst occurring 100 meters outside its 500 meter CEP might still enable it to destroy its target. A kinetic energy penetrator aimed at a fuel storage tank would required much greater accuracy.

The range of a space transient system is typically on the order of several thousand miles. A Pegasus-based system should have sufficient delivery range to limit the danger to the releasing aircraft from defensive action. It should also have range capability as great or greater than systems currently in use (i.e., cruise missiles) that might be considered to fulfill a similar mission.

Responsiveness is an operationally important MOE, and describes the time it takes to deliver a weapon to a target following an order to do so. GPRC claims a four hour response capability, but the value is given without definition of start and stop points. Response times should include consideration of time to perform all functions required to deliver the weapon, including planning, sortie generation, aircraft preflight, flight to the drop point, and actual weapon time-of-flight.

1.6 Operational Assumptions

This thesis makes several assumptions regarding operational deployment of a Pegasus-based system:

- the carrier aircraft will consist of currently operational B-52G or H model aircraft
- the weapon will be maintained by USAF personnel
- mission planning and execution will follow existing USAF guidelines for conventional bombing missions, although modification might be required due to the uniqueness of the system.

1.7 Subsequent Chapters

Chapter 2 contains background material on space strike weapons and a description of the Pegasus launch system. Chapter 3 describes the top-down approach and provides a review of physical principles governing the motion of ballistic and space vehicles. Chapter 4 presents a top-down analysis of the problem. Chapter 5 summarizes the research and makes suggestions for further efforts in this area.

II. Background on Space Strike Weapons and the Pegasus Space

Launch Vehicle

This chapter presents background material relevant to the research, and is divided into two sections. The first section briefly summarizes previous ideas on space strike weapons and surveys the international law concerning the use of space for military applications. It concludes by showing how the concept of force application from space fits into current USAF strategy. The second section is concerned with describing the Pegasus space launch system to include its design philosophy, hardware and mission profile. The section concludes with a discussion of the modifications required for conversion of Pegasus to the space strike role.

2.1 Perspectives on Space Strike Weapons

2.1.1 History The concept of attacking ground targets from above is not new. "Seeking the high ground" has been a tactical goal since the advent of warfare. The age of flight has extended this high ground to the sky, and it is on the verge of being extended into space. In World War II Swiss engineer Eugen Saenger developed a design for what he termed an "antipodal bomber"; a winged vehicle which would be launched on a ballistic trajectory towards its target. Once it began to reenter the atmosphere it would release its payload, pull up aerodynamically ("skip") back into space, and continue to perform such maneuvers around the planet until it could return to its base (20:225). After the war, U.S. interest in this type of vehicle was evidenced by projects like the Bomber-Missile ("BOMI"), Robot Bomber ("ROBO"), and "DYNA-SOAR", a hypersonic weapons system created by the famed Lockheed "skunk works". Technological problems prevented any of these ideas from development, although research into this type of design is ongoing in the form of the National Aerospace plane (NASP).

One space strike weapon that may actually have been fielded was the Soviet Union's "Fractional Orbital Bombardment System", or FOBS. First tested in 1967, the system was apparently designed as an attempt to give the USSR the capability to strike U.S. targets from the south where warning capability was minimal. Armed with a nuclear warhead, the FOBS would be launched into a south orbital trajectory

from the USSR, traverse the South Pole, and reenter the atmosphere prior to its first revolution in order to hit its target. In spite of only limited testing, there were indications that the system may have been partially deployed until the late 1970s (17:99).

The most recent effort in the space force application arena has been in the area of ballistic missile defense, specifically the Strategic Defense Initiative (SDI). Any crossover from its purpose of missile defense to application in the area of force application from space will likely be limited to technology improvements such as miniaturization of guidance hardware

2.1.2 International Law and Agreements Since the beginning of the "space age" in 1957, the international community has persistently expressed the desire to avoid an arms race in the exoatmosphere. A review of relevant documents reveals focus on two primary concerns: banning weapons of "mass destruction" from space, and prohibiting antisatellite (ASAT) weapons.

The first major treaty dealing with space was the 1967 "Treaty on principles governing the activities of states in the exploration and use of outer space, including the Moon and other celestial bodies", commonly referred to as the "Outer Space Treaty". Article IV of this document deals with the weapons of mass destruction issue by outlawing such weapons generally, and nuclear weapons particularly, from Earth orbit or on any celestial body (4:215). The treaty was signed by all United Nations (UN) members and is still in force. The second Strategic Arms Limitations Treaty (SALT II) tried to extend the prohibition specifically to FOBS-type systems but still has not been ratified by the U.S.

The concern over ASAT systems has been expressed in a number of treaties. The SALT I agreement, adopted by both the U.S. and USSR in 1972, prohibits interference with "national technical means of verification" (4:229) and implies the safety of missile warning satellites. The International Telecommunications Convention in 1973 passed an agreement that prohibits "harmful" radio interference by any nation's satellites to any other's (4:29).

None of the above agreements make any statements regarding non-mass destruction weapons in space. As a result, there is no specific restriction on the development and deployment of conventionally armed space strike weapons. The only attempts at doing so were made by the Soviet Union in the form of a pair of proposed treaties

that have yet to be adopted. The first, presented in 1981, stated that weapons of any kind may not be placed in orbit, or on celestial bodies, or on "*reusable manned space vehicles of an existing type or of other types which (might be developed) in the future*" (emphasis added) (4:243). The timing of the proposal, and the obvious reference to the U.S. Space Transportation System, attempted to restrict what the Soviets believed was an intended use of the Shuttle. The second Soviet proposal, presented in 1983, was essentially the same as the 1981 document, except that the reference to reusable manned space vehicles was removed but included that no weapons of any kind could be placed in orbit with the intent of striking objects "on the Earth, in the atmosphere, or in outer space" (4:245). Once again, the timing of the proposal revealed that its true purpose was to prevent U.S. deployment of SDI-based ballistic missile defenses, although if passed it would also have precluded all other types of space strike weapons.

2.1.3 Concurrence with Air Force Strategy There has been a general lessening of the Soviet threat in Europe since 1990, and with this a corresponding attention shift to other regions. A new Air Force strategy concept was presented in 1990 to reflect this. It is termed "Global Reach—Global Power" and contains the following goals for the Air Force:

- to sustain deterrence through nuclear weapons.
- to provide versatile combat forces for theater operations.
- to supply rapid global mobility.
- to control the high ground of space.
- to build U.S. influence among its security partners (8:5).

Space strike weapons have the potential to contribute to the accomplishment of several of these goals. Non-nuclear deterrence could be gained by the ability of such weapons to "maintain constant awareness in potential adversaries that they are always within our reach" (8:3). An ability to strike high value targets with precision, on short notice, and with virtually no risk to friendly forces could most certainly contribute to theater operations. Space control could also be assisted through the denial of launch capability to potential adversaries. The psychological effect might be even greater than the physical effect of such weapons if opponents were subjected to "bolt from the blue" attacks they could not defend against.

2.2 The Pegasus Space Launch System

2.2.1 Overview OSC's Pegasus is a "3 stage, solid propellant, inertially guided, all-composite winged vehicle that is launched at an altitude of 40,000 feet from its carrier aircraft" (5:5.31). It was designed to deliver into orbit the same payloads possible with conventional, fixed launch systems at a lower cost and with great flexibility. The velocity required to achieve orbit was reduced by the following means:

- taking advantage of the velocity imparted by its carrier aircraft
- achieving improved propulsion efficiency through a combination of higher specific impulse caused by lower air pressure at the launch altitude and optimized first stage performance throughout its burn time
- lowering weight due to reduced drag and lower stress of launch at altitude
- minimizing gravity loss due to lift generated by the vehicle's wing (5:5.31).

2.2.2 System Description Pegasus contains four main elements: a carrier aircraft, airborne support equipment, ground support equipment, and the winged booster (5:5.33).

Test flights of Pegasus have used the NASA B-52 aircraft, serial number 00S, which has in the past supported programs such as the X-15 in the 1960s. OSC plans to employ a commercial L-1011 aircraft for post-1993 launches (13:2-8).

Airborne support equipment consists of a launch panel operator (LPO) console and a pylon adapter. The LPO console incorporates a computer, a display, an inertial measurement unit (IMU), an uninterruptable power supply (UPS), and a receiver for telemetry sent from the vehicle (5:5.35). The pylon adapter ensures adequate support for Pegasus' 41,000-pound (plus payload) launch weight (5:5.31).

Ground support equipment includes the following:

- an assembly and integration trailer (AIT) and motor dollies
- transport equipment for delivery, loading, and unloading
- integration test equipment
- payload environmental control equipment (i.e., clean room) (13:6-8).

The winged booster (Figure 1) contains five components: solid rocket motors (one per stage), a payload fairing, a delta wing, an avionics section, and an aft skirt assembly (13:2-2). The solid rocket motors are provided by Hercules Aerospace and

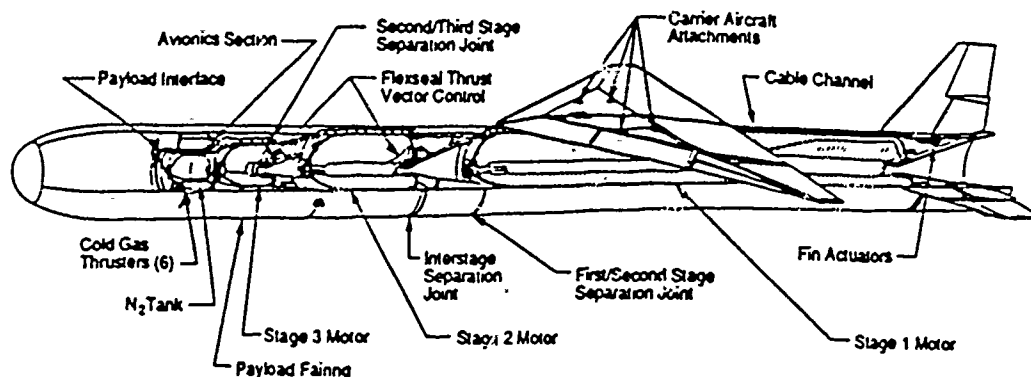


Figure 1. Pegasus Cutaway Drawing (reproduced from (5:5.33))

are "fully flight qualified" (13:2-2). The fairing houses the payload and protects it from damage during ascent. The wing is an all-composite delta of 264-inch span and provides primary lift during the ascent phase. The aft skirt assembly provides aerodynamic flight control. Finally, the avionics system monitors and controls the vehicle throughout the mission. It contains an inertial measurement unit (IMU), a flight computer and autopilot, and a 6-channel Global Positioning System (GPS) receiver for navigation (13:2-7).

2.2.3 Pegasus Mission Profile A typical Pegasus mission (Figure 2) includes four phase points:

- first stage ignition 5 seconds after drop
- a pull-up maneuver during stage 1 burn, followed by stage 2 ignition and burn
- a coasting period during which the payload fairing is ejected
- stage 3 burn to achieve orbit insertion (5:5.36).

Mission profile data is provided the autopilot prior to launch, and attitude control is accomplished via the wing and fins (first stage), and a combination of thrust vectoring and cold-gas roll control (second and third stages) (5:5.34-5.36). OSC

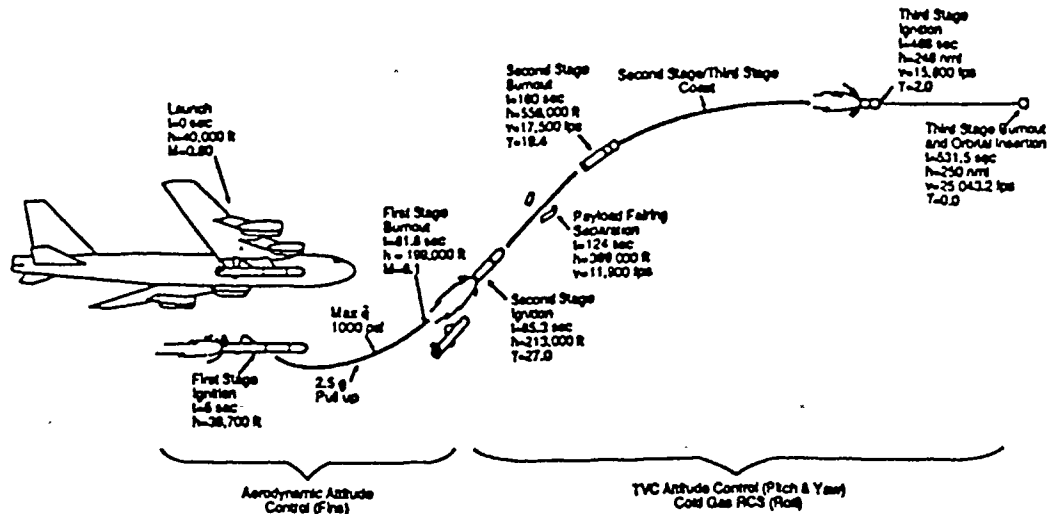


Figure 2. Typical Pegasus Mission Profile (reproduced from (5:5.36))

literature indicates that the vehicle can deliver payloads in excess of 600 pounds into a 200-nautical mile circular orbit if launched from the Cape Canaveral area, and over 800 pounds into a circular equatorial orbit from Kourou, French Guyana (13:3-4).

2.2.4 Adaptations for Space Strike Missions OSC's *Pegasus Payload User's Guide* reveals a distinct emphasis on orbital capability, with only 3 of over 50 pages describing "suborbital and hypervelocity mission profiles" (13). Modifications required for the space strike role would probably reduce system complexity, however. The baseline Pegasus vehicle does not require any modifications to enable it to perform ballistic missions. The OSC material uses a 2-stage vehicle in its ballistic profile, but there is no indication that the full 3-stage vehicle is prohibited from use (13:9-1). Significant checkout is required for an orbital payload due to the many subsystems on board. The payload envisioned for a Pegasus weapon system would most likely consist of "simple" weapons devoid of many complicated electronics. Checkout of the payload should therefore be somewhat quicker and less involved than for a typical satellite. Adaptation of the design to operational B-52 aircraft should present few problems since feasibility of B-52 launch is a demonstrated fact.

2.3 Chapter Summary

A review of the history of space strike weapons indicates a continuing military interest in using space to achieve an advantage in terrestrial conflicts. Current US and USAF space policy seems to lean toward a non-nuclear means of doing so. A Pegasus-based system is one option available to US policy makers, as it would be a space-transient weapons delivery system that could carry a conventional payload. From a historical, political, and operational perspective, the Pegasus option appears to be feasible and worthy of further consideration.

III. Research Method and Analysis Foundations

This chapter contains three sections. The first describes the method of "top-down" analysis and illustrates how it differs from the traditional "bottom-up" approach. The second section presents fundamental physical concepts and principles that are central to analysis of vehicles that travel in or through space. The third briefly describes some terms and relations necessary for analysis of solid-fuel rockets.

3.1 Top-Down Analysis

The process of analysis usually starts when a decision maker poses a question to his analysis shop. He desires their assistance in helping him to make a decision which might only require a simple "yes" or "no". The analysts then attempt to model the process that the decision is based upon, typically proceeding along the following lines:

- a perception of reality is formed, usually in great detail to ensure "realism"
- data requirements are established for all possible factors, starting at the lowest, most detailed level
- as much data as possible is collected, or developed based on some set of assumptions
- a model is then created that successively aggregates lower level modules into higher levels until all possible interactions are accounted for
- voluminous output is generated and converted into charts, graphs, and tables
- the results are presented to the decision maker, who is left to make his decision without much insight into the factors that really drive the output (7:2).

This analysis approach might be called a "bottom-up" approach because it starts at the lowest possible system level and works up. A high level of detail is attained, and the model used to determine the results is large and complex. Output of the model usually includes many pages of digitized data "accurate" to several decimal places. The "answers" provided, however, are the end results of a model that tries to reproduce reality rather than answer a specific question.

The models that define reality are limited to the range of available data, and if no data are available, they are subject to whatever assumptions the analysts make regarding them. The decision maker's choice must therefore be based on a very narrow range of possibilities within the "space" defined by all feasible outcomes. Figure 3 illustrates this concept with the axes representing a pair of system components. The values of factor (B) are constrained by the availability of data to the indicated range, while a lack of information has forced the analyst to "fix" the value of factor (A). Factor interactions are therefore limited to a very small range of possibilities.

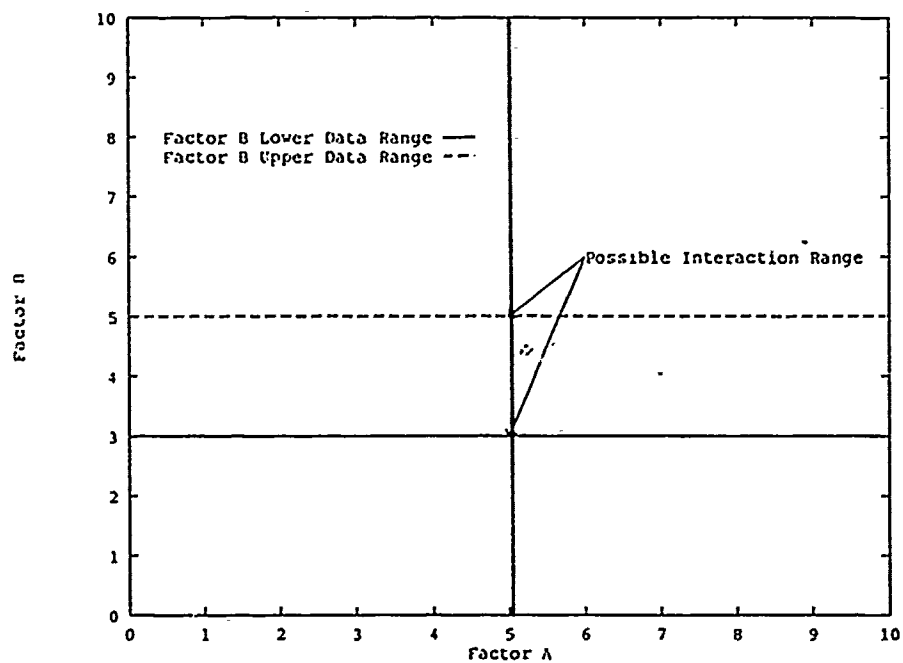


Figure 3. Traditional Analysis Decision Space

Attempting to accurately model "reality" presents its own problems. First, the analyst's perception of reality may be wrong from the outset, or it may omit one or more essential elements. Second, the model might either be so large that it takes considerable time to run or so complex that it is very difficult to change. An analyst faced with a short suspense might try to fit a new problem into an existing model not originally designed to accept it. Even if a current problem can be made to fit an existing model, there is the possibility that the assumptions on which the model is based make it unsuitable. As a result, any "answers" determined by the analysis

shop might be highly precise and detailed, but completely irrelevant to the decision that must be made. Finally and perhaps most importantly, since the model was not designed around the decision, management cannot see what factors truly drive the results, and must attempt to derive for themselves any insight into the effects of changing them.

Data problems associated with the bottom up approach are also significant. Detailed data is very costly to collect or develop, either in terms of time or money or both. Data may not even exist if conceptual designs are being evaluated. Finally, computer-generated digital output presents its own unique problems; results might be given 'accurately' to ten decimal places, although the input data may have been correct to only one or two (7:3).

A "top-down" analysis is designed from the decision maker's point of view. The formalized method was developed by the Science and Technology Research, Inc. (STR), and is generally performed as follows:

- the *final decision* is examined to determine the fundamental questions that must be answered for the decision to be correct
- each question is analyzed to determine the critical issues and components that affect it. The decision maker should be extensively involved at this point to determine his view of the "big picture" as it involves these essential factors
- potential solutions to the problem are developed, and each alternative evaluated for the *lowest level of detail* that sufficiently describes it
- first-order analyses of the alternatives are made to identify the most influential drivers
- sensitivity and trade-off analyses are conducted around these essential drivers
- the results of the analysis are presented as a series of "curves" rather than "point estimates", enabling the decision maker to see clearly the implications of alternative choices (6:2).

The analyst performing a top-down analysis must always approach the problem from the decision maker's point of view. The first step in the approach entails the definition of the decision space within which the decision maker will make his choice. The axes that define this space correspond to the most important issues

that affect the decision. Two- or three-dimensional subspaces are formed for all possible factor combinations, and trade offs between factors are presented as a series of curves (or surfaces) corresponding to different levels of assumed performance. A decision maker's mission concept will define the necessary range required for a positive decision, and such graphs clearly show him not only *how* he should answer, but *why*. Figure 4 shows a typical two-factor graph, with the vertical and horizontal lines representing the minimum acceptable performance level of each factor as defined by the decision maker. The performance curves correspond to factor level pairs

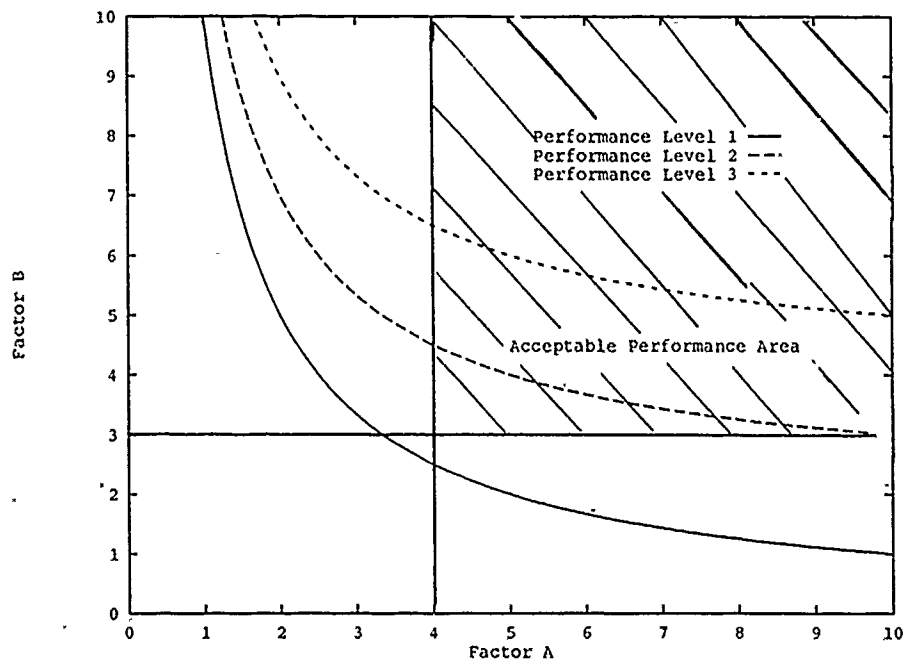


Figure 4. Typical Top-Down Analysis Decision Space

necessary to achieve these requirements. The factors that define the decision space are aggregations of lower level factors, parameters, or drivers. Each lower-level factor is subjected to its own "mini analysis" aimed at identifying its essential drivers, and the results of each of these is given as a set of curves. This process is repeated until all factors significantly influencing the ultimate decision have been identified (7:3). The top-down approach avoids or greatly diminishes many of the problems associated with the bottom-up approach. Data problems are minimized because the level of detail is typically much less in the top-down than in the bottom-up

approach. Estimates of parameter bounds are usually much easier to obtain than exact values and allow for a wider variety of possibilities. Also, assumptions are "numerous and explicit" (7:4), allowing for analysis into sensitivity of the results to changing parameter values. In addition, since the analysis is performed around the decision, risk of irrelevancy is minimized. Finally, the decision maker can see for himself what issues are most essential to the decision. He can "back into" the assumptions he must make about specific factors if he makes a particular decision. He can then use his own judgement to decide if the assumptions are reasonable, or he can direct further, more detailed analysis on *pertinent and specific* factors that he desires more information on.

A feasibility study is a good candidate for a top-down analysis effort. A mission concept is developed and a system chosen for potential application, but the system either does not exist or has not been employed in the manner desired. As a result, data are very difficult to obtain. A top-down approach used to determine driving factors can be of great use as a "bridge" between those deciding whether to pursue a given system (the decision makers), and those that are able to determine the hardware capabilities of the system (the engineers). The study can serve as a focus for both groups; the decision maker can specify a certain level of performance and know what requirements must be obtained, and the engineers can see the areas in which to concentrate their efforts in order to attain the specified requirements. Each succeeding layer in the analysis serves as a filter for the system; if at any point the system cannot meet the performance requirement, no further analysis is needed to address the fundamental question. If the original requirements are not attainable, both groups will be able to see what is possible with the hardware capabilities that can be attained. The analyst in this situation is in effect an arbitrator, ensuring the concerns from both sides are effectively addressed.

This thesis is essentially a feasibility study. The underlying question driving it is: "Should a space-strike system based on the Pegasus launch vehicle be pursued?" A traditional approach to answering this problem might be to incorporate the engineering specifications of Pegasus into a simulation of possible ballistic strike missions. Various warhead designs might be tried and random variation of system parameters injected so as to produce an "answer" to the question. There are several problems with this approach. First, Pegasus has never been used in a ballistic profile and has performed less than a dozen orbital delivery missions. Parameter variability

assumptions would therefore be based on a less-than-statistically significant number of flights. Also, assumptions regarding warhead design specifications quickly raise the required level of security classification above unclassified. A classified analysis requires secure processing and limits the ability to gather valuable input from outside sources. Finally, there would likely not be insight into the parameters that drive the final results.

The top-down approach to the problem is presented in Chapter 4. The original decision is broken into fundamental questions that define the essential decision space. Each of these axes forms a "track" down which successive layers of detail are added until the essential system drivers are determined.

3.2 Fundamentals of Space Flight Analysis

This section is divided into four subsections: introduction, basic relationships, ballistic trajectory analysis, and perturbations.

3.2.1 Introduction The fact that the planets travel in elliptical paths about the sun was discovered by Kepler in 1609, and the mathematics that describe the motion were developed by Newton later in the seventeenth century (1:3). Objects that are launched from the earth into orbit also follow elliptical paths around the earth. Ballistic missiles exhibit the same motion, save that the "orbits" they follow happen to intersect the surface of the earth. There are many forces that act on a vehicle that determine the precise characteristics of its orbit, but not all have the same degree of influence. The earth's gravity exerts by far the greatest effect on orbital (and ballistic) vehicles. Gravitational fields of the Sun and the Moon are also influential, as are atmospheric drag, the non-spherical nature of the earth, solar radiation, magnetic effects, and the effects of relativity (1:386).

This section first presents the coordinate frames commonly used for near-earth orbits. The parameters required for analysis are described next, followed by basic equations describing parameter relationships. Third, specific issues of interest in ballistic trajectory analysis will be presented.

3.2.1.1 Assumptions. The effects listed above (gravity et.al.) all serve to alter, or *perturb*, a theoretical orbit. The "ideal" conditions assumed in this research are a spherical, non-rotating earth and resultant uniform inverse-square

gravitational field. The earth is not an ideal system, so the equations given here are often modified in practice. Appendix C describes some of these, although they are not essential to this research.

3.2.1.2 Reference Frames. There are numerous reference frames in the field of orbital mechanics, but the one that is used in this study is known as the "geocentric-inertial" frame (1:55) (see Figure 5). This frame exhibits the desirable

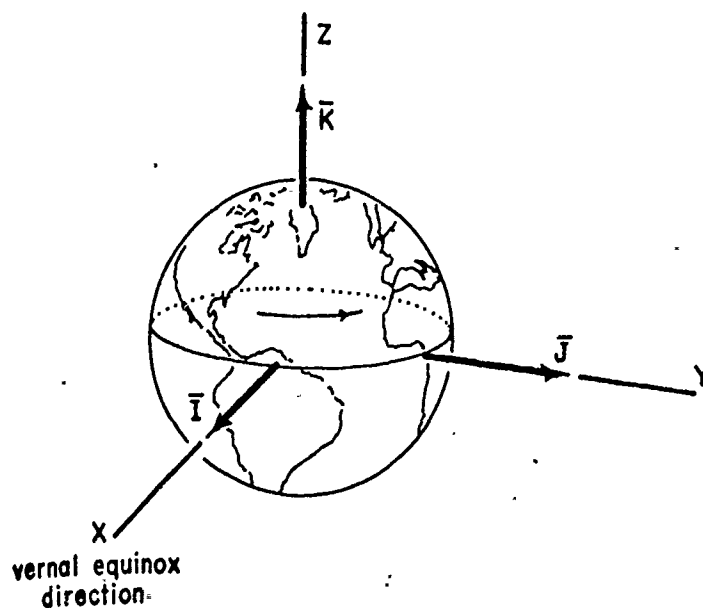


Figure 5. Geocentric-Equatorial Coordinate System (reproduced from (1:55))

property of maintaining its orientation while the earth rotates. The center of the coordinate system is the center of the earth, the x and y axes lie in the plane of the equator, and the z axis runs through the north pole. The positive- x direction is fixed and points in the direction of the star Aries no matter where the earth is in its orbit around the sun. Vector notation is commonly used in orbit analysis, and to this end the $\vec{i} - \vec{j} - \vec{k}$ unit vectors have been established by convention to correspond with the $x-y-z$ axes

3.2.1.3 Definition of Parameters. There are six parameters, referred to as "orbital elements", that serve to fully define any given orbit. They are illustrated in Figure 6 and described below. The long axis of the ellipse, called the "major

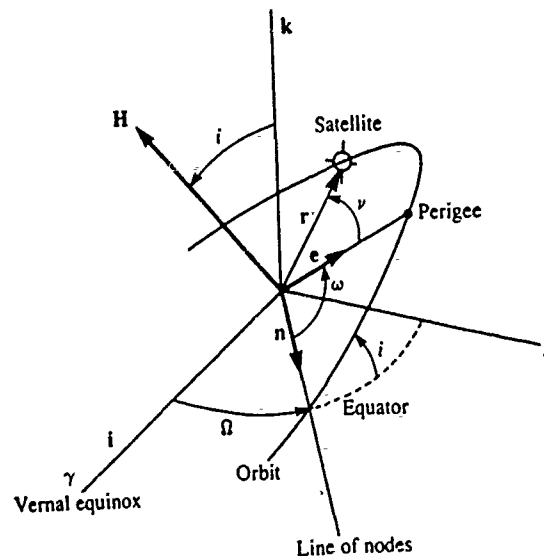


Figure 6. Orbital Elements (reproduced from (20:58))

axis", contains the center and both foci. The semi-major axis (denoted ' a ') is the parameter that represents the distance measured from the center of the ellipse to the farthest point on the orbit away from the center. This point is called the *apoapse*. The short or "minor axis" is defined by the line joining the center with the point on the orbit closest to the center. It is perpendicular to the long (major) axis and ends at the point of *periapse*. Eccentricity (denoted ' e ') is a measure of orbit shape, with possible value greater than or equal to zero. Table 1 details the relation between eccentricity value and shape. Inclination (denoted ' i ') orients the orbit with respect to the equator, and is measured as a positive angle up from the equator. The ascending node is the point at which a vehicle crosses the equatorial plane from south to north, and the parameter associated with it is defined by the longitude at which it occurs (denoted ' Ω '). The line joining the center of the earth with the ascending node defines the "line of nodes". The angle measured in the orbit plane between the line of nodes and the major axis is called the "argument of perigee" (denoted ' ω '). Finally, the time at which the vehicle first crosses periapse is given a parameter, T . There are a few special cases in the use of these parameters:

- if the orbit plane lies in the equatorial plane, there is no ascending node and Ω is undefined

<i>e value</i>	<i>conic</i>
0	circle
$0 < e < 1$	ellipse
1	parabola
$e > 1$	hyperbola

Table 1. Eccentricity-Orbit Shape Relationship

- if the orbit is circular, there is no perigee and ω is undefined (1:60).

The values of three additional parameters are determined by the vehicle itself (see Figure 7). The position and velocity of the vehicle at any time in its orbit are given by the vectors \vec{r} and \vec{v} . The \vec{r} vector is measured from the center of the earth to the orbiting vehicle's center of mass, and the \vec{v} vector is measured along the vehicle's centerline in the direction of flight. The third parameter is called the *flight path angle*, denoted by the Greek letter ϕ , and is the angle measured from the "local horizontal" (which is always orthogonal to the radius vector) to the velocity vector.

A final parameter describes the range of a ballistic trajectory. It is common to see ballistic missile ranges given in terms of distance (nautical miles, kilometers, etc.), but this study expresses them mostly as angles. The *total range angle* is denoted by the Greek symbol Λ , and is the angle measured from the center of the earth that includes the launch and target points. This angle is further sub-divided into three parts corresponding to a specific phase of flight for a ballistic trajectory: powered flight (boost), free-flight, and re-entry. The symbols Γ , Ψ , and Ξ are used to represent each of these, and their sum is the value of Λ .

3.2.2 Basic Relationships The equations involved in orbit analysis have been derived for the most part from analytical geometry. These fundamental geometric equations are listed without derivation, as such information can be found in many mathematics texts. Basic mechanics principles are also be listed, and the derivation can be found in (1:16-18).

3.2.2.1 Geometry Equations. The following describe the relation between the semi-major axis (a), eccentricity (e), and the magnitude of the radius vector (r).

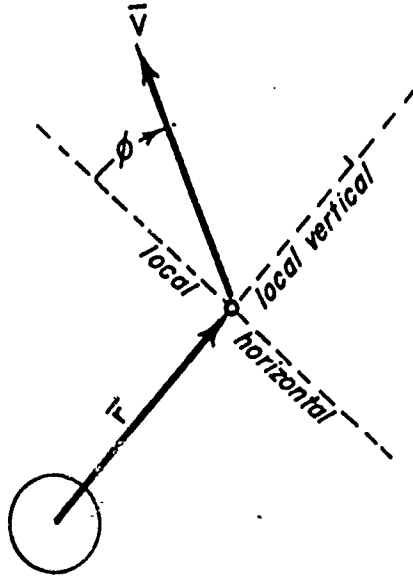


Figure 7. Vehicle Dependent Parameters (reproduced from (1:17))

The equation in polar coordinates for any conic section is given by

$$r = \frac{a(1 - e^2)}{1 + e \cos \nu} \quad (1)$$

where ν is the angle from periapse (perigee in the geocentric coordinate system) to the radius vector.

If the distance from the center of the earth to apoapse (apogee) is r_a and to periapse is r_p , then the eccentricity of the conic is given by

$$e = \frac{r_a - r_p}{r_a + r_p} \quad (2)$$

An additional term often used in orbital analysis defines the distance perpendicular to the major axis which is measured from a focus to the orbit. It is called the *semi-latus rectum*, or "parameter", and is denoted p . Its value may be determined

by using Eq (1) with $p = r$ and $\nu = 90^\circ$:

$$p = a(1 - e^2) \quad (3)$$

This term will enable easier manipulation of subsequent equations.

3.2.2.2 Mechanics Equations and Time of Flight Calculation. This section presents physics-based equations describing the motion of a vehicle in an inverse-square gravitational field such as that generated by the earth. The *period* of an orbit is the term used to describe the time a vehicle takes to complete a single orbit, and equations are given to determine this value.

Newton's law of universal gravitation relates the force exerted on one mass by another. It can be expressed in equation form as

$$\vec{F} = -\frac{Gm_1m_2}{r^3}\vec{r} \quad (4)$$

where \vec{F} is the force, \vec{r} is the vector from m_1 to m_2 , r is the magnitude of this vector, and G is the universal gravitational constant.

The mass of a typical space vehicle is negligible compared to that of the earth, so the vehicle's mass can be ignored in the equation. This results in the simplified expression

$$\vec{F} = \frac{GM_e}{r^3}\vec{r} \quad (5)$$

where M_e is the mass of the earth.

The term GM_e occurs often in practice and will be denoted by the symbol μ , termed the "earth's gravitational constant" and having the value (1:429)

$$\mu = 3.986012 \times 10^5 \frac{\text{km}^3}{\text{sec}^2} \quad (6)$$

The two other physical properties that most significantly affect a space vehicle's motion are conservation of energy and conservation of momentum, both of which remain constant in a uniform gravitational field (1:14). Conservation of energy can

be expressed by the equation

$$\mathcal{E} = \frac{v^2}{2} - \frac{\mu}{r} \quad (7)$$

where \mathcal{E} is the *specific mechanical energy* of the vehicle and v is the magnitude of the velocity vector (1:16). The principle of conservation of momentum gives rise to the equations

$$\vec{h} = \vec{r} \times \vec{v} \quad (8)$$

and

$$h = rv \cos \phi \quad (9)$$

where \vec{h} is the *angular momentum vector*, h is its magnitude, and ϕ is the flight path angle (1:17-18). The value of h is a maximum when $\phi = 0$, and this occurs at both apogee and perigee.

The above conservation equations can be related to the fundamental geometric equations, as shown in the following example (1:20-29). At the point of perigee, $\phi = 0$. Letting the subscript p represent the values at perigee, $r = r_p$, and from Eq (9), $h = r_p v_p$. Equation (7) then becomes

$$\mathcal{E} = \frac{h^2}{2r_p^2} - \frac{\mu}{r_p} \quad (10)$$

Using Eq (1) and the fact that $h^2/\mu = a(1 - e^2)$, Eq (10) can be further reduced (1:20) to:

$$\mathcal{E} = -\frac{\mu}{2a} \quad (11)$$

Lastly, vector integration of the two-body motion equation gives the following (1:19-20):

$$p = \frac{h^2}{\mu} \quad (12)$$

This equation can be combined with Eq (9) to get

$$p = \frac{r^2 v^2 \cos^2 \phi}{\mu} \quad (13)$$

Time of flight determination is made using Kepler's second law which states that the radius vector "sweeps out equal areas in equal times" (1:2). The area swept

in one orbit is the total area of the ellipse, given by

$$\text{area} = \pi ab \quad (14)$$

where a and b are the lengths of the semi-major axis and semi-minor axis, respectively. This may be developed into the following equation for orbital period (1:31-33):

$$\mathcal{P} = \frac{2\pi}{\sqrt{\mu}} a^{3/2} \quad (15)$$

One additional term, known as the *eccentric anomaly* and denoted E , is required for time calculations. A circle circumscribed about an ellipse will have a radius equal to the length of the semi-major axis (a). A line drawn through any point on the ellipse perpendicular to the major axis will intersect the circle as well. The eccentric anomaly is the angle subtended at the center of the ellipse by the major axis and the ray from the center to the intersection point on the circle. This angle can be used to develop the following equation for time of flight determination (1:183-185):

$$t_p - T = \sqrt{\frac{a^3}{\mu}} (E - e \sin E) \quad (16)$$

where T is the time of periapse passage and $t_p - T$ is the time of flight from periapse to some point p in the orbit. This equation may also be derived from the following relationship, which will be more useful in responsiveness analysis (1:185):

$$\cos E = \frac{e + \cos \nu}{1 + e \cos \nu} \quad (17)$$

3.2.3 Ballistic Trajectory Analysis A ballistic trajectory is composed of three phases, *boost*, *free-flight*, and *re-entry* (1:279). The point of intersection between the boost phase and free-flight phase is called the *burnout point*, and the free-flight phase is separated from the re-entry phase by the *re-entry point*. Figure 8 illustrates the phases of flight, intersection points, and corresponding range angles, and also the vehicle-dependent parameters \vec{r} , \vec{v} , and ϕ at the burnout point. The figure shows that the shape of the free-flight phase defines the orbit characteristics of the trajectory. The theoretical impact point would occur at the location where this "orbit" intersects

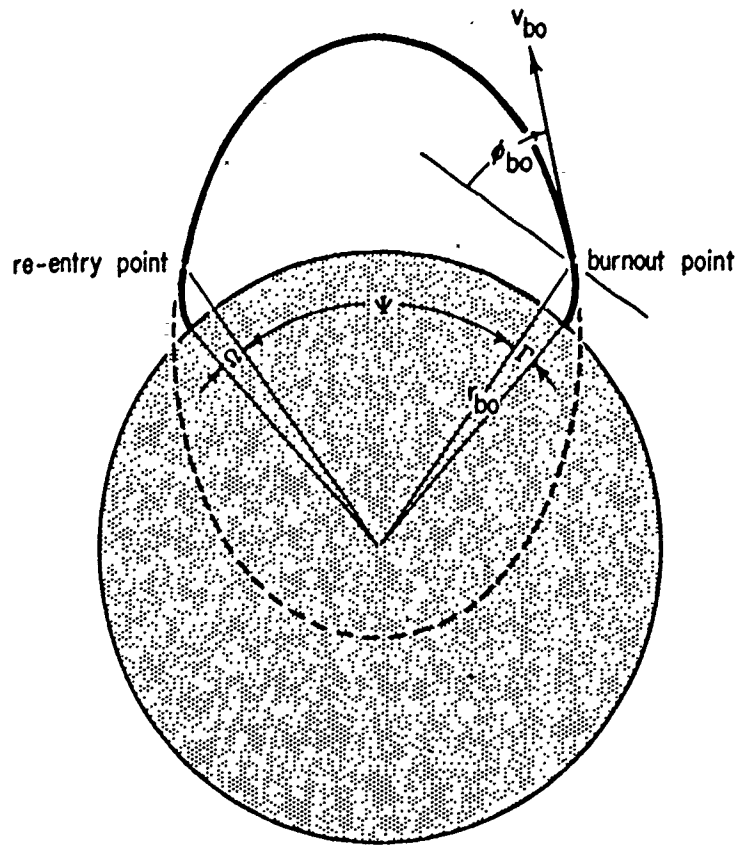


Figure 8. Ballistic Trajectory Phases (reproduced from (1:281))

the surface of the earth. Table 2 lists the primary forces that act on a vehicle in each phase.

The following sections develop the equations necessary for performance analysis of a vehicle following a ballistic trajectory. The basic relationships between the range of the trajectory and the position, speed, and flight path angle of the vehicle at the burnout point are developed first, followed by a discussion of parameter value errors and their effects on the theoretical equations.

3.2.3.1 Range Angle Determination. The subsequent derivations concentrate on the determination of free-flight range, Ψ . The powered flight phase is of interest primarily at the burnout point, since parametric values at this point define the character of the remaining portion of the trajectory. The re-entry phase trajectory is assumed to simply follow that of the nominal free-flight trajectory.

<i>phase</i>	<i>physical forces</i>	<i>means of control</i>
boost	gravity, aerodynamic	on-board sensors, rocket thrust
free-flight	gravity	control jets (if present)
re-entry	gravity, aerodynamic	warhead-dependent

Table 2. Forces Acting on a Ballistic Trajectoried Vehicle

This leads to the corresponding assumption that if the re-entry point occurs at the planned location, the vehicle will hit the target.

Subsequent analysis assumes a trajectory symmetric about the major axis. Figure 9 shows the results of such an assumption, with the subscript *bo* indicating a burnout value, and *re* indicating a re-entry value. A symmetric trajectory occurs if the vehicle is unpowered during the free-flight phase. Typically, a warhead bus (the platform that holds the re-entry vehicle(s) until its designated drop point(s)) incorporates some limited maneuver capability. The initial trajectory determined by the burnout conditions would be changed after each maneuver, and the new trajectory would then follow the symmetric path defined by the changed parameters.

A convenience parameter, Q , is used to simplify the equations associated with orbit mechanics. It is defined as (1:280):

$$Q = \frac{v^2 r}{\mu} \quad (18)$$

Substituting this equation into Eq (7) and Eq (10) yields

$$a = \frac{r}{2 - Q} \quad (19)$$

Rearranging terms gives

$$Q = 2 - \frac{r}{a} \quad (20)$$

Since the trajectory is symmetric about the point of apogee, $\Psi/2 + \nu_{bo} = 180^\circ$. Thus,

$$\cos \frac{\Psi}{2} = -\cos \nu_{bo} \quad (21)$$

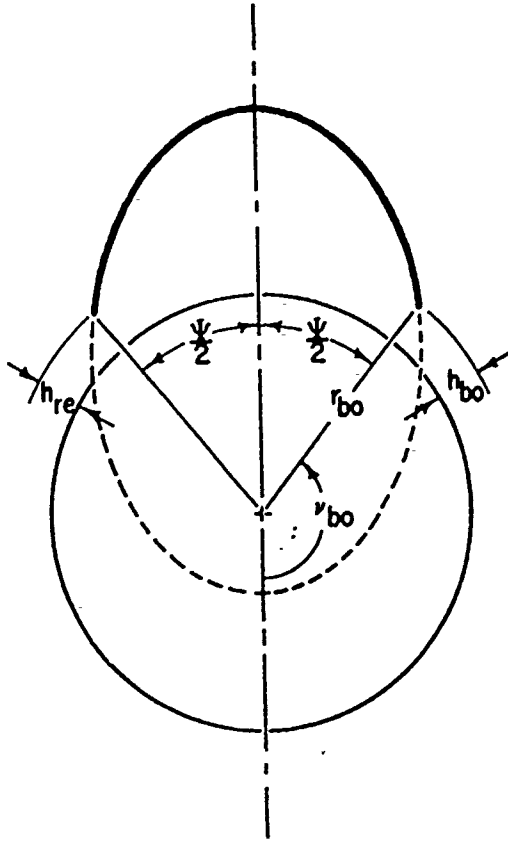


Figure 9. Symmetry Effects (reproduced from (1:283))

Combining this with Eq (1) and solving for $\cos \Psi/2$ yields

$$\cos \frac{\Psi}{2} = -\cos \nu_{bo} = \frac{r_{bo} - a(1 - e^2)}{er_{bo}} \quad (22)$$

Using Eq (13) and the definition of Q ,

$$p = rQ \cos^2 \phi \quad (23)$$

Finally, combining Eqs (19), (22), and (23) yields the "free-flight range equation" (1:284):

$$\cos \frac{\Psi}{2} = \frac{1 - Q_{bo} \cos^2 \phi_{bo}}{\sqrt{1 + Q_{bo}(Q_{bo} - 2) \cos^2 \phi_{bo}}} \quad (24)$$

This equation is useful for determining free-flight range for any set of burnout conditions and can determine the theoretical impact point of a re-entry vehicle.

Calculating the effects of parameter errors requires differentiation of this equation implicitly with respect to its different variables. Hence, a more readily differentiated form is now presented (1:286).

Equation (24) represents a right triangle relationship. From trigonometry, if A is an angle in a right triangle, a is the length of the adjacent side, and b is the length of the hypotenuse, then

$$\cos A = \frac{a}{b} \quad (25)$$

Similarly,

$$\cot A = \frac{a}{\sqrt{b^2 - a^2}} \quad (26)$$

As the numerator of Eq (24) corresponds to a and the denominator to b in Eq (25), it may therefore be expressed in the manner given by Eq (26):

$$\cot \frac{\Psi}{2} = \frac{1 - Q_{bo} \cos^2 \phi_{bo}}{Q_{bo} \cos \phi_{bo} \sqrt{1 - \cos^2 \phi_{bo}}} \quad (27)$$

Since $\sqrt{1 - \cos^2 \phi_{bo}} = \sin \phi_{bo}$ and, in general, $\cos a \sin a = 1/2 \times \sin 2a$, then Eq (27) can be further simplified to

$$\cot \frac{\Psi}{2} = \frac{2}{Q_{bo}} \csc 2\phi_{bo} - \cot \phi_{bo} \quad (28)$$

Rearranging terms results in the following equation, useful in subsequent error analysis:

$$\cot \frac{\Psi}{2} = \frac{2\mu}{v_{bo}^2 r_{bo}} \csc 2\phi_{bo} - \cot \phi_{bo} \quad (29)$$

3.2.3.2 Flight Path Angle Determination. Given fixed vehicle position and speed, the flight path angle needed to achieve a given range may be determined.

Figure 10 illustrates the geometry behind the derivation of the subsequent equations, used to calculate flight-path angle. In this figure, F and F' are the foci of the elliptical orbit, and r'_{bo} is the line joining the burnout point to F' . Geometry

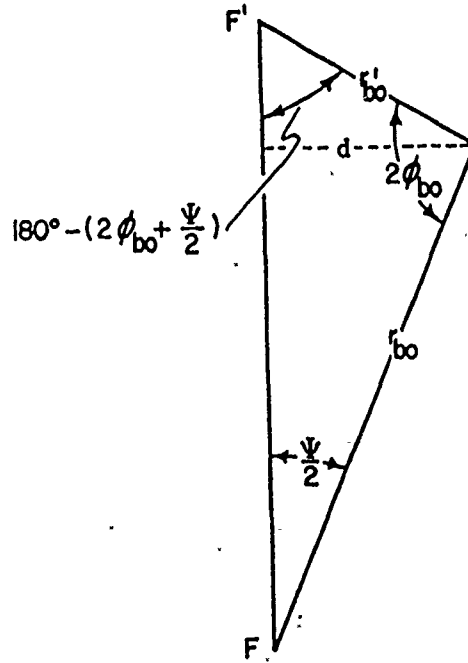


Figure 10. Ellipse Geometry (reproduced from (1:287))

yields the following relationships:

$$d = r_{bo} \sin \frac{\Psi}{2} \quad (30)$$

and

$$d = r'_{bo} \sin \left(180^\circ - \left(2\phi_{bo} + \frac{\Psi}{2} \right) \right) \quad (31)$$

Using Eqns (30) and (31), the fact that $\sin(180^\circ - x) = \sin x$, and the fact that

$$r_{bo} + r'_{bo} = 2a \quad (32)$$

results in the "flight-path angle equation":

$$\sin \left(2\phi_{bo} + \frac{\Psi}{2} \right) = \frac{2 - Q_{bo}}{Q_{bo}} \times \sin \frac{\Psi}{2} \quad (33)$$

Examination of Eq (33) leads to the realization that for all values of r , v , and Ψ , there are *two* possible values of ϕ owing to the nature of the sine function. The greater value is termed the *high trajectory* and the lesser is called the *low trajectory* (1:287). Relating the possible values of ϕ_{bo} to those of Q_{bo} leads to the relationship between the vehicle parameters and maximum range. If $Q_{bo} < 1$, then both trajectories are possible, although there will be a theoretical maximum range. If $Q_{bo} = 1$, then one of the trajectories will represent a circular orbit that skims the earth and is not practical. If $Q_{bo} > 1$, then one of the trajectories will be negative, and thus also impractical. This last case, however, leads to ranges in excess of 180° , and represents the theoretical foundation of the "fractional orbital bombardment system (FOBS)" mentioned in Chapter 2.

The maximum range for a given value of Q_{bo} may be determined by setting the right side of Eq (33) to "1" and solving for Q_{bo} :

$$\sin \frac{\Psi}{2} = \frac{Q_{bo}}{2 - Q_{bo}} \quad (34)$$

The minimum Q_{bo} value necessary to achieve a given maximum range may be determined by rearranging terms and solving for Q_{bo} :

$$Q_{bo} = \frac{2 \sin \frac{\Psi}{2}}{1 + \sin \frac{\Psi}{2}} \quad (35)$$

3.2.3.3 Effects of Parameter Errors on Impact Location. This section describes how errors at the burnout point affect the predicted re-entry point. There are two types of error, called "down-range" and "cross-range" (1:297), which are the result of incorrect parameter values at burnout, incorrect burnout location, or both. Down-range error arises as the result of displacement of the intended burnout location in the nominal trajectory plane and deviation of the r , v , and ϕ parameters from the planned values. Cross-range error is due to lateral displacement (out of the nominal trajectory plane) of the burnout point and deviation from the planned vehicle azimuth at burnout.

The effect of in-plane displacement of the burnout point is easiest to evaluate, since any such deviation produces a like deviation at the impact point. Therefore, if the burnout point occurs 1 km farther downrange than planned, the re-entry point

will be 1 km farther downrange. The resulting impact location will also show a like deviation unless the re-entry vehicle has a degree of maneuverability. The remaining factors are somewhat more difficult, requiring implicit differentiation of the free-flight range equation (Eq (29)).

The expression representing the total down-range error due to incorrect parameter values may be written mathematically as

$$\Delta \Psi_{Total} = \frac{\delta \Psi}{\delta r_{bo}} \times \Delta r_{bo} + \frac{\delta \Psi}{\delta v_{bo}} \times \Delta v_{bo} + \frac{\delta \Psi}{\delta \phi_{bo}} \times \Delta \phi_{bo} \quad (36)$$

where the first, second, and third terms of the right-hand side represent the effects due to small errors in the burnout point (r in effect represents altitude), the burnout velocity, and the burnout flight-path angle, respectively (1:305).

Differentiating of Eq (29) with respect to r_{bo} yields

$$-\frac{1}{2} \csc^2 \frac{\Psi}{2} \delta \Psi = \frac{-2\mu}{v_{bo}^2 r_{bo}^2} \csc 2\phi_{bo} \delta r_{bo} \quad (37)$$

Solving for $\delta \Psi / \delta r_{bo}$ and rearranging terms results in

$$\frac{\delta \Psi}{\delta r_{bo}} = \frac{4\mu}{v_{bo}^2 r_{bo}^2} \frac{\sin^2 \frac{\Psi}{2}}{\sin 2\phi_{bo}} \quad (38)$$

which expresses range-angle deviation due to small errors in burnout height.

To determine the effects of burnout velocity error, differentiation of Eq (29) with respect to v_{bo} yields

$$-\frac{1}{2} \csc^2 \frac{\Psi}{2} \delta \Psi = \frac{-4\mu}{v_{bo}^3 r_{bo}} \csc 2\phi_{bo} \delta v_{bo} \quad (39)$$

Solving for $\delta \Psi / \delta v_{bo}$ and rearranging terms results in

$$\frac{\delta \Psi}{\delta v_{bo}} = \frac{8\mu}{v_{bo}^3 r_{bo}} \frac{\sin^2 \frac{\Psi}{2}}{\sin 2\phi_{bo}} \quad (40)$$

giving range-angle error due to small velocity error.

A final differentiation of Eq (29) with respect to ϕ_{bo} yields the range-angle error due to small flight-path angle deviation:

$$-\frac{1}{2} \csc^2 \frac{\Psi}{2} \delta \Psi = \frac{2\mu}{v_{bo}^2 r_{bo}} (-2 \cot 2\phi_{bo} \csc 2\phi_{bo}) \delta \phi_{bo} + \csc^2 \phi_{bo} \delta \phi_{bo} \quad (41)$$

Combining Eqs (29) and (41) and solving for $\delta \Psi / \delta \phi_{bo}$ leads to

$$\begin{aligned} -\frac{1}{2} \csc^2 \frac{\Psi}{2} \frac{\delta \Psi}{\delta \phi_{bo}} &= -2 \cot 2\phi_{bo} \left(\cot \frac{\Psi}{2} + \cot \phi_{bo} \right) + \csc^2 \phi_{bo} \\ &= -2 \cot 2\phi_{bo} \cot \frac{\Psi}{2} - 2 \cot 2\phi_{bo} \cot \phi_{bo} + \csc^2 \phi_{bo} \\ &= -2 \cot 2\phi_{bo} \cot \frac{\Psi}{2} - \left(\frac{2 \cos 2\phi_{bo} \cos \phi_{bo}}{\sin 2\phi_{bo} \sin \phi_{bo}} \right) + \frac{1}{\sin^2 \phi_{bo}} \\ &= -2 \cot 2\phi_{bo} \cot \frac{\Psi}{2} - \left(\frac{\cos 2\phi_{bo}}{\sin^2 \phi_{bo}} \right) + \frac{1}{\sin^2 \phi_{bo}} \\ &= -2 \cot 2\phi_{bo} \cot \frac{\Psi}{2} + \left(\frac{1 - \cos 2\phi_{bo}}{\sin^2 \phi_{bo}} \right) \\ &= -2 \cot 2\phi_{bo} \cot \frac{\Psi}{2} + 2 \\ &= 2 \left(1 - \cot 2\phi_{bo} \cot \frac{\Psi}{2} \right) \end{aligned}$$

Continuing,

$$\begin{aligned} \frac{\delta \Psi}{\delta \phi_{bo}} &= 4 \left(\cot 2\phi_{bo} \sin \frac{\Psi}{2} \cos \frac{\Psi}{2} - \sin^2 \frac{\Psi}{2} \right) \\ &= 2 \cot 2\phi_{bo} \sin \frac{\Psi}{2} \cos \frac{\Psi}{2} - 4 \left(\frac{1 - \cos 2(\frac{\Psi}{2})}{2} \right) \\ &= 2 \left(\frac{\cos 2\phi_{bo} \sin \Psi}{\sin 2\phi_{bo}} + \cos \Psi \right) - 2 \\ &= 2 \frac{\cos 2\phi_{bo} \sin \Psi + \cos \Psi \sin 2\phi_{bo}}{\sin 2\phi_{bo}} - 2 \end{aligned}$$

which finally results in the desired relationship:

$$\frac{\delta \Psi}{\delta \phi_{bo}} = \frac{2 \sin(\Psi + 2\phi_{bo})}{\sin 2\phi_{bo}} - 2 \quad (42)$$

The deviations that contribute to cross-range errors are straightforward in evaluation, as there are no derivatives involved. Analysis of these errors, due to out-of-plane displacement of the burnout point and to incorrect launch azimuth, requires only the use of spherical trigonometry and the small angle approximation

$$\cos \alpha \approx 1 - \frac{\alpha^2}{2} \quad (43)$$

It is assumed for this discussion that the free-flight range angle travelled by the vehicle is the same on the actual trajectory as on the intended one (i.e., there are no parameter errors). In the case of an incorrect launch azimuth, the burnout point is correct but the re-entry point is divergent from the intended. In the case of an out-of-plane displacement of the burnout point, the vehicle will still move towards the intended re-entry point due to the spherical nature of the earth, but unless the intended range angle was 90° , it will either undershoot or overshoot. In either case, the impact point is likely to be displaced from the intended by some distance corresponding to an arc with length dependent on the angle it subtends at the center of the earth. In Figure 11, if there is a lateral displacement of the burnout point ΔC , then the impact point will be displaced by $\Delta\beta$. Similarly, if the launch azimuth is off by $\Delta\beta$, then the impact will occur at a point ΔC from the intended impact point.

To determine the error, the law of cosines for spherical trigonometry is used in the form appropriate to the specific type of error. For the burnout point displacement case, this is

$$\cos \Delta\beta = \sin^2 \Psi + \cos^2 \Psi \cos \Delta C \quad (44)$$

Assuming only a small error, then Eq (44) may be used and the above may be simplified as follows:

$$\begin{aligned} \left(1 - \frac{\Delta\beta^2}{2}\right) &\approx \sin^2 \Psi + \cos^2 \Psi \left(1 - \frac{\Delta C^2}{2}\right) \\ &\approx (\sin^2 \Psi + \cos^2 \Psi) - \cos^2 \Psi \frac{\Delta C^2}{2} \\ &\approx 1 - \cos^2 \Psi \frac{\Delta C^2}{2} \end{aligned}$$

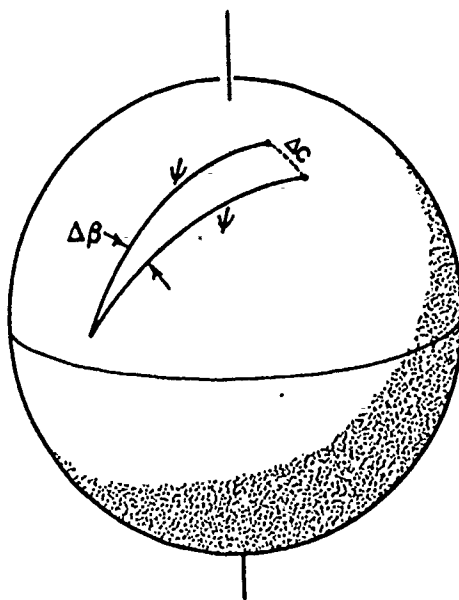


Figure 11. Cross-range Error Analysis (reproduced from (1:299))

This can be reduced to

$$\Delta\beta^2 \approx (\cos^2 \Psi) \Delta C^2 \quad (45)$$

which results in

$$\Delta\beta \approx \Delta C \cos \Psi \quad (46)$$

For the case of incorrect launch azimuth, the appropriate form of the cosine law gives

$$\cos \Delta C = \cos^2 \Psi + \sin^2 \Psi \cos \Delta\beta \quad (47)$$

Assuming only a small error, Eq (43) may be used to result in

$$\Delta C \approx \Delta\beta \sin \Psi \quad (48)$$

As mentioned, range angles close to 90° are least sensitive to lateral burnout point displacement, but conversely most sensitive to incorrect launch azimuth (1:300).

3.3 Solid Rocket Terms and Relations

Several basic terms are used in this thesis to establish bounds on expected performance capabilities of the Pegasus launch system. The *mass ratio* (denoted MR) of a solid rocket stage is the vehicle mass remaining after the stage has ceased operating but prior to stage separation (denoted m_f), divided by the initial mass of the vehicle (denoted m_o). In equation form this is expressed by

$$MR = m_f/m_o \quad (49)$$

Propellant *specific impulse* (denoted I_s) is the primary performance parameter for a rocket propellant, and is dependent on the specific chemicals used in its formulation. The *effective propellant exhaust velocity* (denoted v_e) is the velocity at which the propellant is ejected from the rocket and is determined by the equation

$$v_e = I_s g_o \quad (50)$$

where g_o is the effective gravitational acceleration (18:22-23).

The total velocity attained by a multistage rocket like Pegasus is the sum of the velocities imparted by each stage. The maximum theoretical velocity "gain" (denoted Δv) by a given stage is given by the equation

$$\Delta v = v_e \ln \frac{1}{MR} + v_o, \quad (51)$$

where v_o is the initial velocity before rocket operation. This maximum velocity is found by assuming ideal operating conditions - no gravity and operation in vacuum (18:99-103).

3.4 Chapter Summary

This chapter introduced the top-down analysis approach and contrasted it with a "traditional" approach. The top-down approach was shown to be superior in terms of focusing analysis efforts on the decision at hand, reducing data requirements, unveiling hidden assumptions, and identifying driving factors. The chapter also presented the astrodynamics concepts and equations that form the theoretical basis

for space flight analysis. Both of these are used in Chapter 4 to assess whether Pegasus can serve as an effective weapons delivery vehicle.

IV. Top-Down Performance Analysis

This chapter presents a top-down approach to the decision of pursuing a potential Pegasus-based strike system. The essential factors contributing to the decision are broken down into successively more detailed components until all drivers have been identified.

4.1 Overview

A decision to pursue development of a Pegasus-based ballistic space strike system is dependent on the system's ability to achieve minimum acceptable performance levels in several areas. This thesis presumes these to be delivery range in kilometers, target destruction probability, and response timeliness in hours. Each of these factors defines an axis in the possible decision space which combine to form a three-dimensional coordinate system. The eventual decision of whether to pursue the issue is dependent on acceptable performance capability along all three of these decision "axes". Each of these axes gives rise to a distinct "track" for analysis. The top-down approach dictates that each "layer" in this analysis describe the principal determinants of performance of the immediately preceding layer. The following sections outline the principal determinants of the three performance criteria considered in this study.

4.1.1 Trajectory Range According to Eq (24), ballistic trajectory range is determined by the burnout point values of flight-path angle (ϕ_{bo}), altitude (r_{bo}), and velocity magnitude (v_{bo}), the latter two combining to yield the convenience parameter, Q . The possible values for Pegasus delivery range are therefore a function of the burnout parameter values that Pegasus is capable of achieving. Figure 12 shows the levels of analysis performed along the range axis.

4.1.2 Probability of Target Destruction The probability that a Pegasus-delivered weapon will destroy a target is a function of both the weapon and the target. Specific combinations of these are not considered, except in the following, general terms. The weapon is assumed to be non-nuclear; therefore the "lethal area" in which it can damage a target is relatively small. Targets are assumed to be fixed in position but varying in size. The analysis presented in this section therefore assumes that

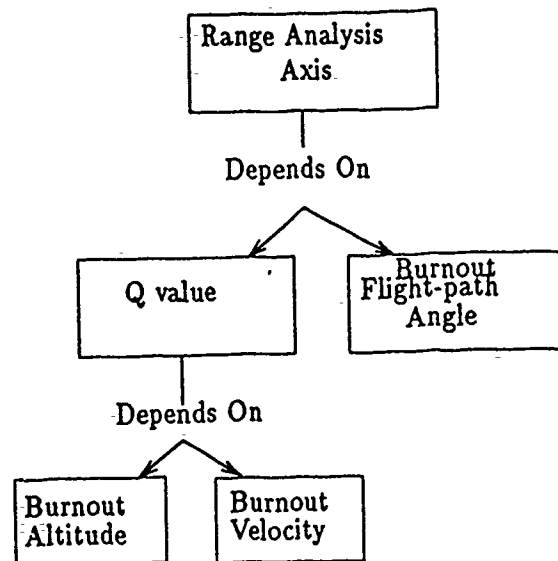


Figure 12. Range Axis Analysis Levels

the weapon must hit the target to be effective, and that if hit, the target is destroyed. Whether a target is hit is then a function of the accuracy of delivery and an appropriate target characteristic. Accuracy is expressed in terms of "circular error probable", or CEP. Size in terms of target radius is used as the "target characteristic", although other factors such as hardness could also be considered. Accuracy is considered herein to be a function of the extent of displacement from a planned re-entry location, expressed as down-range and cross-range error. Chapter 3 shows down-range error to be primarily a function of errors in the planned values of r_{bo} , v_{bo} , and ϕ_{bo} , and cross-range errors to be the result of errors in burnout point location and azimuth. Figure 13 shows the level to which the top-down approach is herein applied to the PD axis.

4.1.3 Pegasus Responsiveness Responsiveness is dependent on the amount of time required for the carrier aircraft to deliver Pegasus to its drop point and the time Pegasus takes to fly to the target. A Pegasus-based system is likely to be much different than any currently in use regarding mission planning and preparation, so analysis of responsiveness dictates a broad range of assumptions. Figure 14 shows the extent of analysis along this track with the topics chosen to give maximum insights.

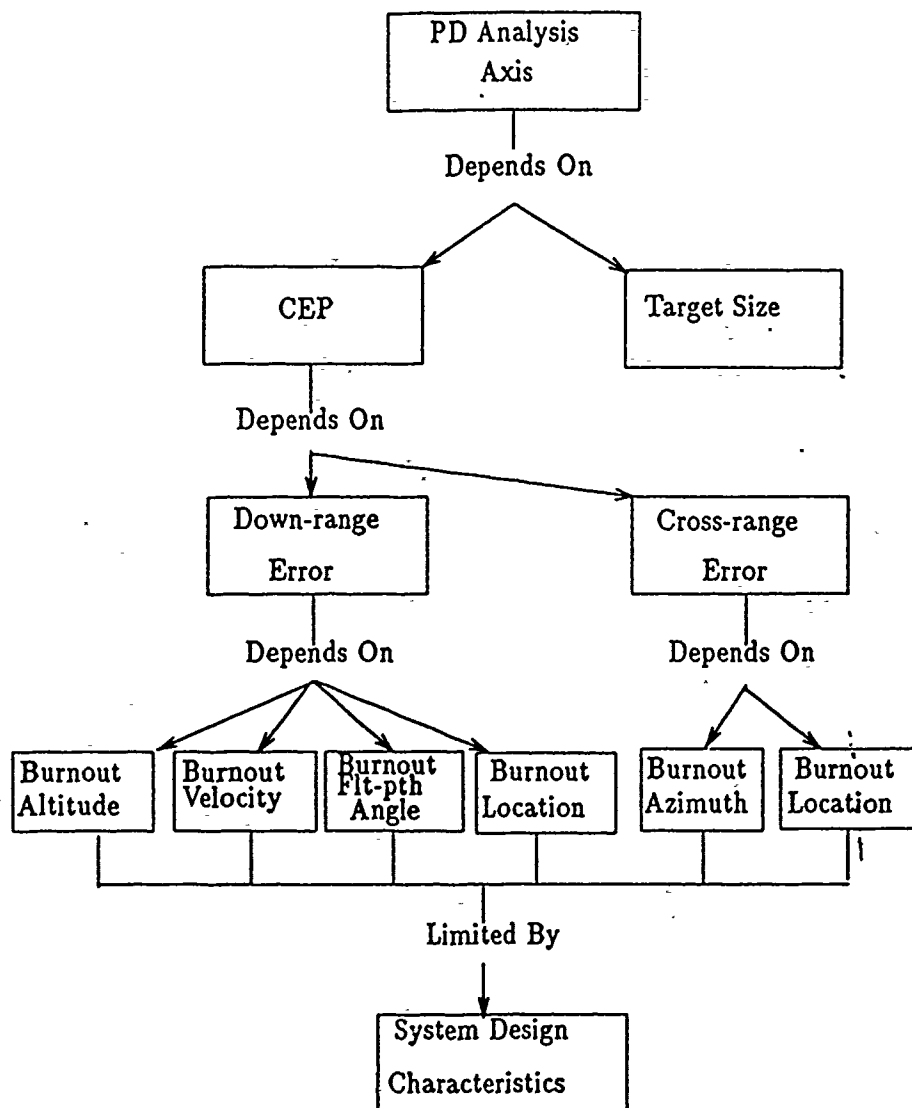


Figure 13. PD Axis Analysis Levels

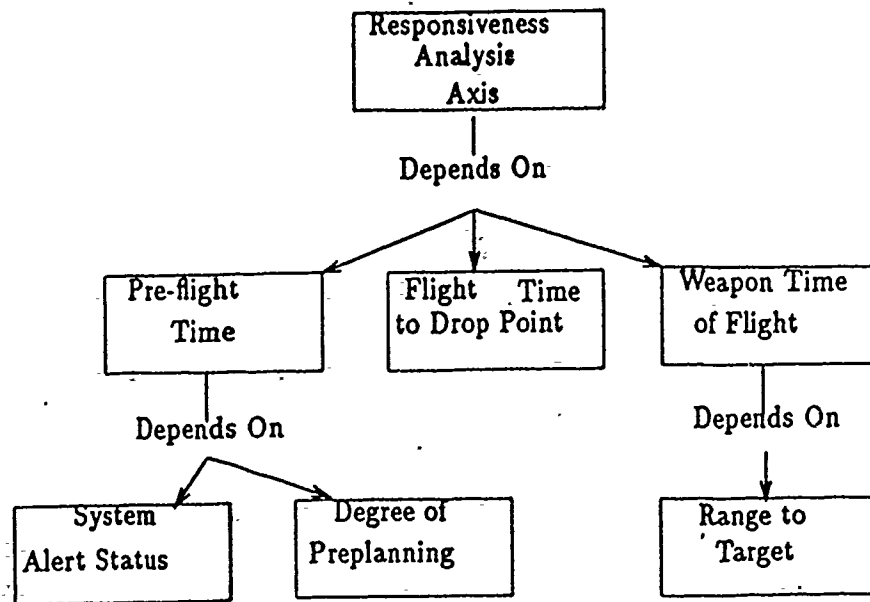


Figure 14. Responsiveness Axis Analysis Levels

4.2 Range Axis Analysis

A top-down approach to delivery range potential begins with the question "If range X is desired, what parameter values are required for Q and ϕ_{bo} ?" Figure 15 shows that there are several combinations of Q and ϕ_{bo} values that combine to yield most of the ranges indicated. Typically, the flight-path angle value is predetermined by the design of the re-entry vehicles (RVs), so a particular range requires a corresponding, specific Q value. The choice of a particular combination of Q and flight-path angle must be made carefully. Chapter 3 introduces the idea of "high" and "low" trajectories, and it can be shown that the high trajectory is generally less sensitive to parameter errors than the corresponding low trajectory for a specified Q and range combination. Appendix B develops this idea in more detail.

Given that a specific Q -value is required, then its constituent factors must be subject to further examination to determine which are most influential. Equation (18) indicates that Q is proportional to the burnout altitude (r_{bo}) and to the square of the burnout velocity (v_{bo}). Figures 16 and 17 show the sensitivity of Q to variations in the individual parameters that determine it. The curves in Figure 16 clearly show that Q varies greatly with a change in v_{bo} . The near horizontal nature of the "curves" in Figure 17 also show that large changes in burnout altitude are

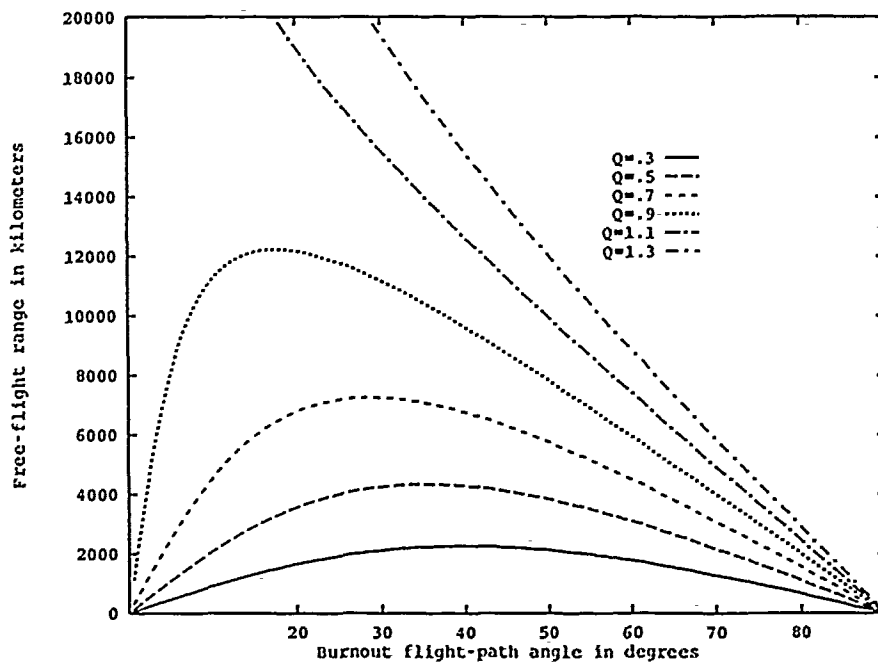


Figure 15. Parameter Requirements for Given Delivery Ranges

relatively insignificant. Burnout velocity magnitude is clearly the driving factor in the determination of Q .

4.3 Target Destruction Axis Analysis

The probability of target destruction (PD) is determined by the effectiveness of a particular weapon against a particular target, assuming that the weapon is delivered accurately enough that its lethal area intersects the target. The weapons under consideration for deployment by Pegasus (KE or conventional explosive) would generate a relatively small lethal area. This thesis assumes that a target of a given size will be "destroyed" if hit by a weapon. The PD is therefore determined by the CEP of the Pegasus-delivered re-entry vehicle and the radius of the target. Figure 18 shows how combinations of CEP and target radius interact to achieve different levels of PD. The curves representing different CEP requirements represent solutions

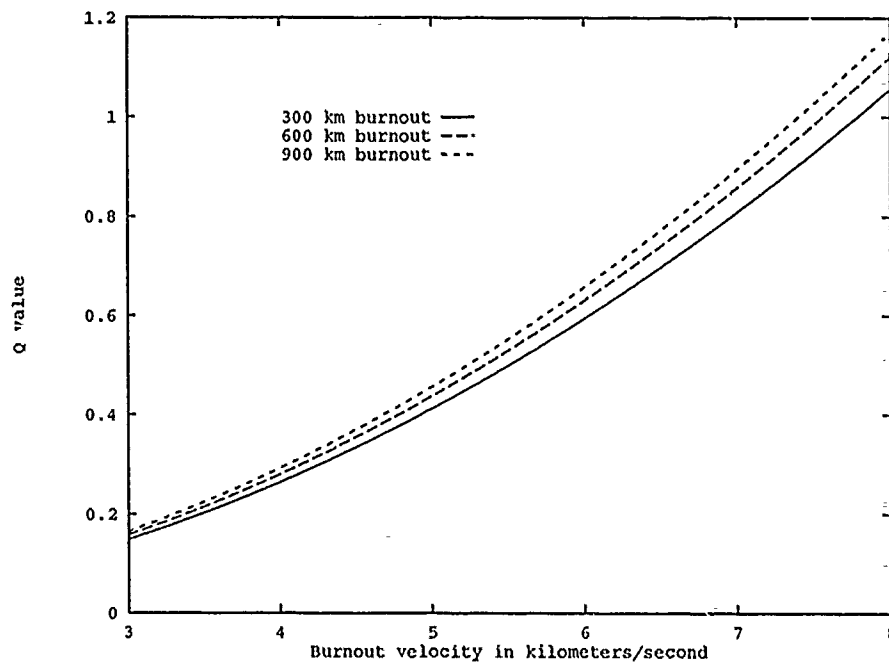


Figure 16. *Q* Value vs. Velocity

to the following equation:

$$CEP \text{ Required} = \frac{\text{target radius}}{\sqrt{\ln(1 - PD)/\ln .5}} \quad (52)$$

This equation is derived from that describing the “probability of striking in a circle of (a given radius)” (19:86). It assumes the “best case” of circular weapon impact dispersion centered on the target.

4.3.1 CEP Determination Further examination of CEP first requires a brief overview of the concepts that determine its value. Two general classes of errors, referred to as “systematic” errors and “random” errors, combine to yield a system’s CEP value. Systematic errors are those that occur consistently as the result of tests repeated under identical conditions. They are the effect of peculiarities of the *system* under study, as well as “assumptions and simplifications of every kind that are made in solving the firing problem” (19:45). The effect of parameter value errors can be considered systematic; changing a parameter by a given amount produces a known

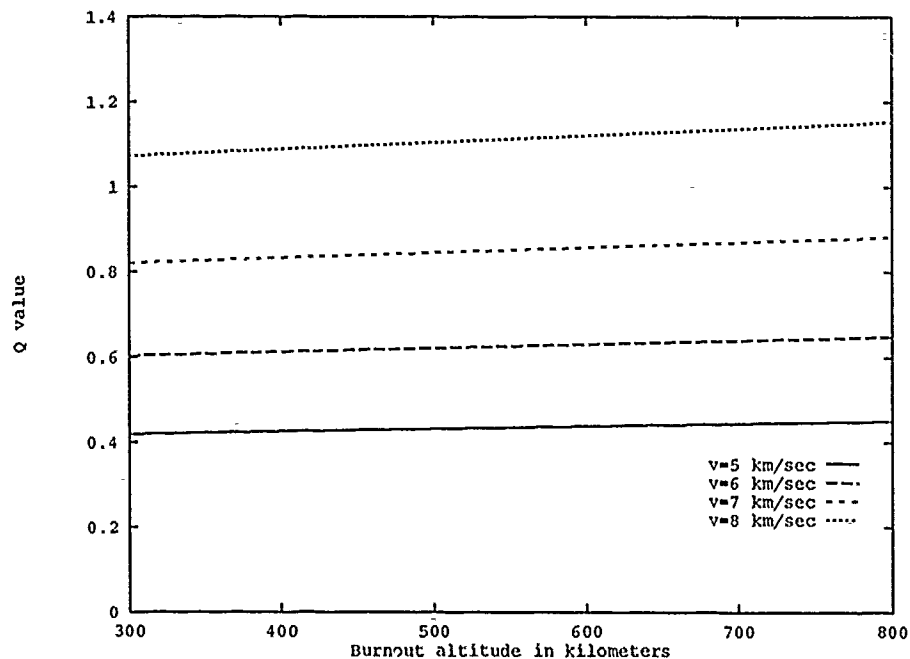


Figure 17. Q Value vs. Burnout Altitude

effect, which can be determined by solving the appropriate equation. Random errors, on the other hand, "vary from shot to shot, *creating a dispersion around the center of the grouping*" (19:45)(emphasis added). Systematic errors define the displacement, or *bias* of the shot group from the intended target location. The center of the grouping defines the *mean point of impact*, or MPI. If the bias is zero, then the MPI is centered on the intended target location. CEP for unbiased (bias=zero) groupings is determined by the extent of the dispersion caused by random error effects. As bias increases, CEP becomes increasingly large until its calculation becomes dominated by systematic error-induced bias, rather than random error-induced dispersion.

The simplest analytical case is that of an unbiased, circular dispersion. In this case, the mean value of down-range and cross-range error (denoted \bar{d} and \bar{c}) is zero (centered on the MPI), and the standard deviations of down-range and cross-range error (denoted S_d and S_c) are equal (2:3-3). Calculation of CEP for circular, unbiased dispersions can be made by the simple equation $CEP = 1.1774S$ (2:A-5), where S is the common standard deviation of both down- and cross-range errors ($S = S_c = S_d$). The next simplest case is that of unbiased, non-circular dispersions. The values of S_d

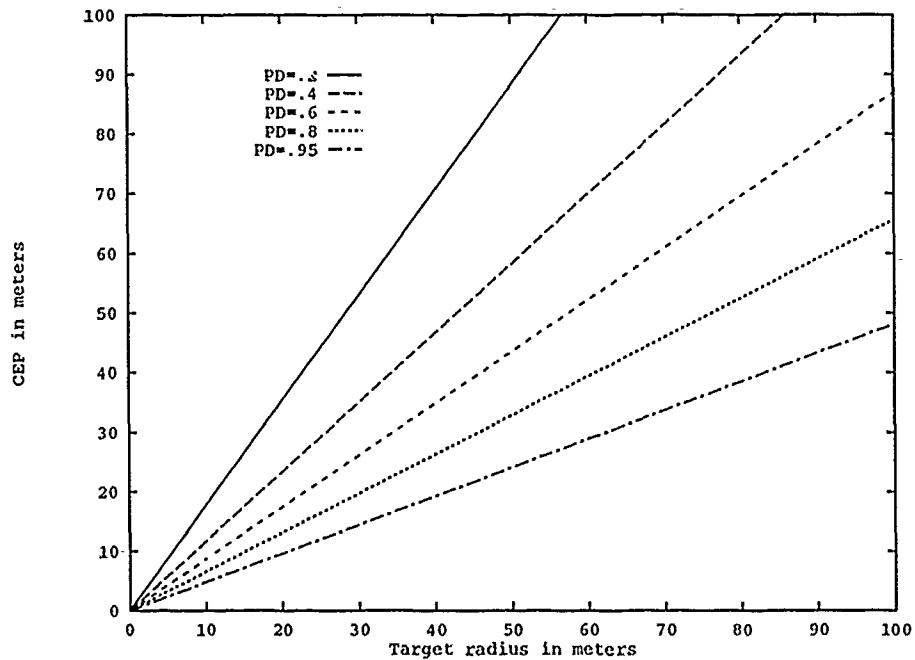


Figure 18. Probability of Destruction: CEP vs. Target Radius

and S_c are not equal, and the “ellipticity” of the dispersion is the ratio of S_c to S_d . Thus, a circular dispersion has an ellipticity of 1.0. CEP calculation for unbiased, elliptic dispersion patterns may be made using the following equation, which has been shown to be valid for ellipticities between 0.25 and 1.0 (2:A-6):

$$CEP = 0.614S_c + 0.563S_d \quad (53)$$

The most difficult case is that of biased dispersion patterns. A variety of approximation techniques are available for CEP calculations under this case, but this thesis will use the following, known as the “Grubbs-Patnaik/Wilson-Hilferty” equation:

$$CEP = \sqrt{m(1 - (k/9m^2)^3)} \quad (54)$$

The variables m and k are defined as follows:

$$m = (S_d^2 + S_c^2 + \bar{d}^2 + \bar{c}^2) \quad (55)$$

$$k = 2(S_d^4 + 2\rho^2 S_d^2 S_c^2 + S_c^4) + 4(\bar{d}^2 S_d^2 + 2\bar{d}\bar{c}\rho S_d S_c + \bar{c}^2 S_c^2) \quad (56)$$

where ρ is the correlation factor between the values of d and c . This factor (ρ) is a measure of the linear relationship between d and c . This thesis assumes $\rho = 0$.

4.3.1.1 Random Error Effects. Defining a certain CEP requirement places constraints on the extent of possible values of all factors involved—bias (\bar{d} and \bar{c}), correlation (ρ), and standard deviations of down- and cross-range errors (S_d and S_c). The smallest CEP occurs if there is zero bias and small dispersion, implying small random errors. The following graphs show the maximum possible values of S_d and S_c to achieve a range of CEPs, assuming zero bias. Figure 19 illustrates the simplest case of a circular dispersion, and Figure 20 demonstrates the elliptic case.

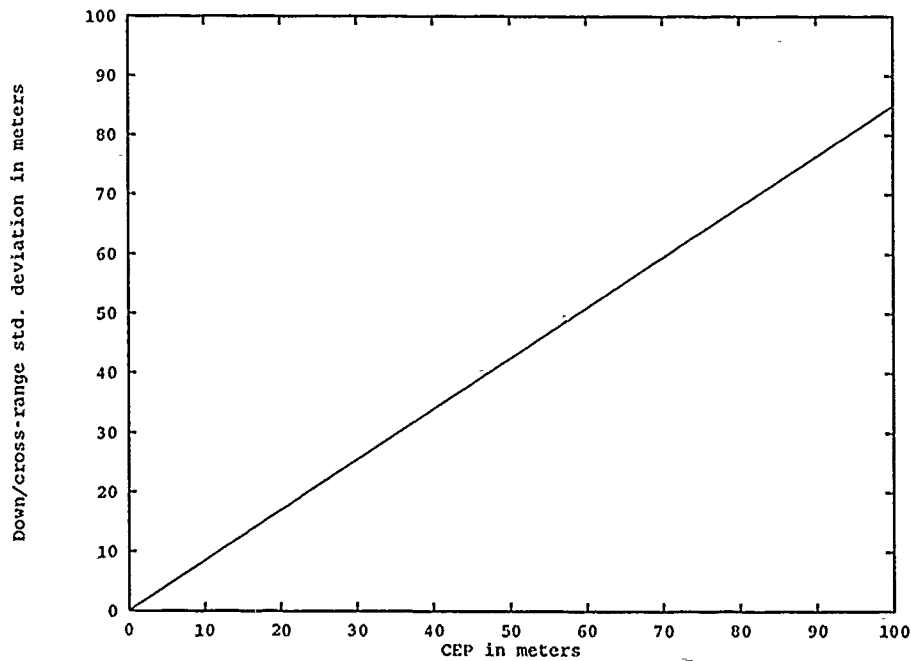


Figure 19. Maximum Down- and Cross-range Standard Deviation: Circular Dispersion

These figures indicate the extent (i.e., the “upper limits”) of random error-induced dispersion for a given CEP. Since the figures assume an MPI centered on the in-

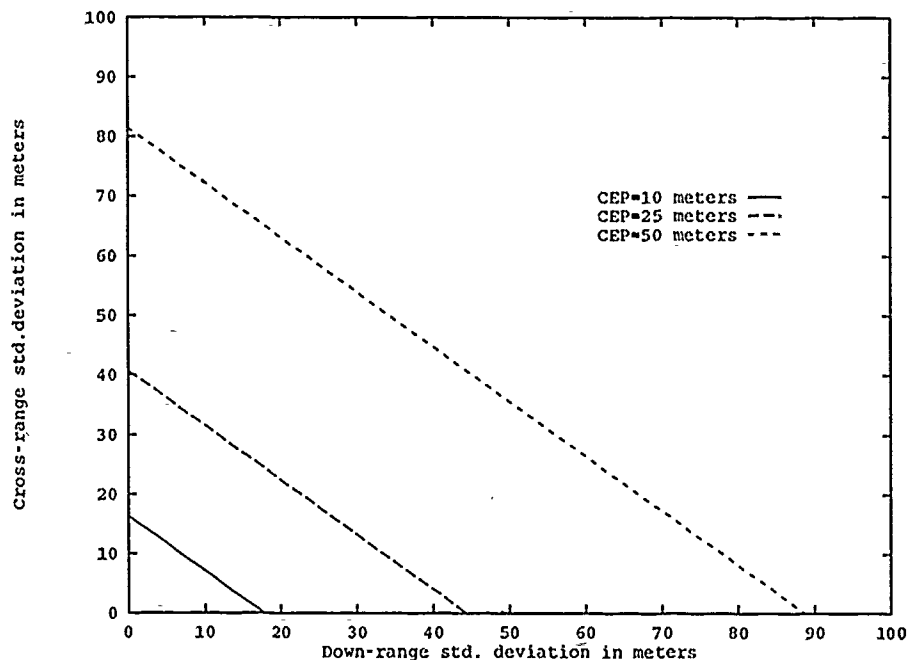


Figure 20. Maximum Down- and Cross-range Standard Deviation: Elliptic Dispersion

tended target, the introduction of systematic bias will reduce the allowable standard deviation below the values given.

4.3.1.2 Systematic Error Effects. Figure 21 shows the effect of introducing bias into CEP calculation, assuming uncorrelated, circular dispersion. The curves are generated by solving Eq (53), where the square of the bias is equal to the sum of the squares of the mean down- and cross-range values; i.e., $b^2 = \bar{d}^2 + \bar{c}^2$. The figure clearly illustrates how the introduction of bias radically affects CEP for standard deviations as small as 10 meters. Thus, controlling system-induced bias is critical to controlling CEP. Since bias is determined by the magnitude of down-range and cross-range error, these must likewise be tightly controlled. Figure 22 shows the extent of allowable down- and cross-range displacement for several bias values. This figure again shows that the constraints on allowable errors are very tight for small bias tolerance.

Down-range and cross-range errors are caused by errors in the planned values of mission parameters. Analysis of the relative effects of each requires the introduction

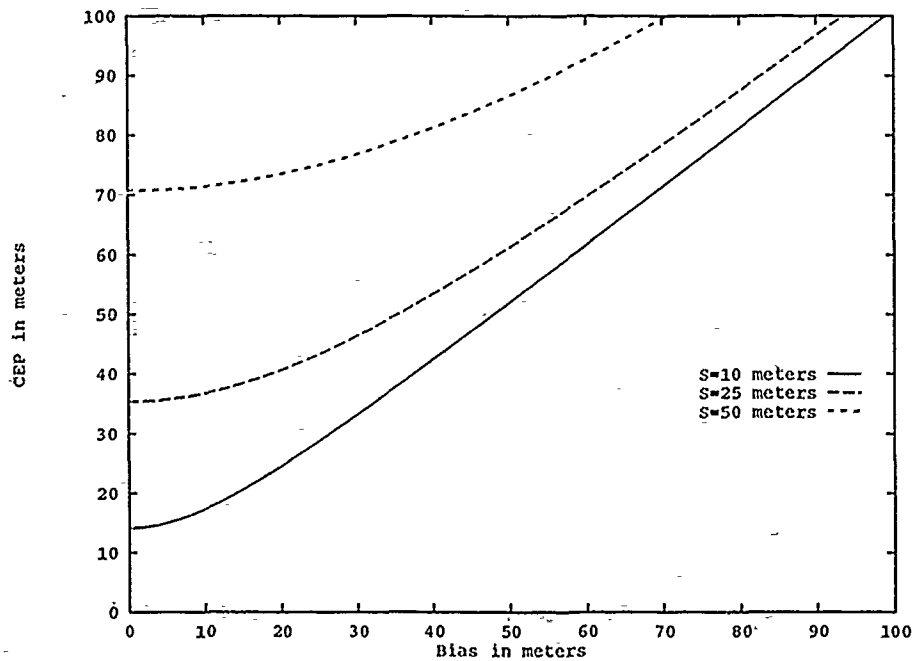


Figure 21. Bias Effects on CEP: Circular Dispersion

of the term "influence coefficient". Influence coefficients for all relevant parameters are derived in Appendix B, with the results summarized in Tables 3 and 4. These tables give a representative range of values based on analysis contained in Appendix B. The re-entry point displacement magnitude is found by multiplying the error magnitude by the appropriate influence coefficient. Figures 23 and 24 show typical displacement due to errors in two of the three parameters determining down-range error, v_{bo} and r_{bo} . The curves represent the interactions between parameters that combine to yield the flight range indicated. The assumed Q value is 0.665, chosen because it is representative of Pegasus performance capability. Appendix B shows how values other than this yield slightly different effects, but the general relationships shown in these figures hold.

If bias is to be held to under 25 meters, v_{bo} must be controlled to within approximately 0.005 meters/second (from Figure 23), and r_{bo} must not be allowed to exceed its intended value by more than approximately 10 meters (from Figure 24).

<i>Parameter name</i>	<i>Down-range displacement per "unit" of error</i>
altitude (r)	1-3 km/km
velocity (v)	1-5 km/(m/sec)
flight-path angle (ϕ)	100-300 km/degree
burnout point displacement (in-plane)	1 km/km

Table 3. Parameter Error Influence Coefficients: Down-range Effects

<i>Parameter name</i>	<i>Cross-range displacement per "unit" of error</i>
azimuth	60-120 km/degree
burnout point displacement (lateral)	0.5-0.9 km/km

Table 4. Parameter Error Influence Coefficients: Cross-range Effects

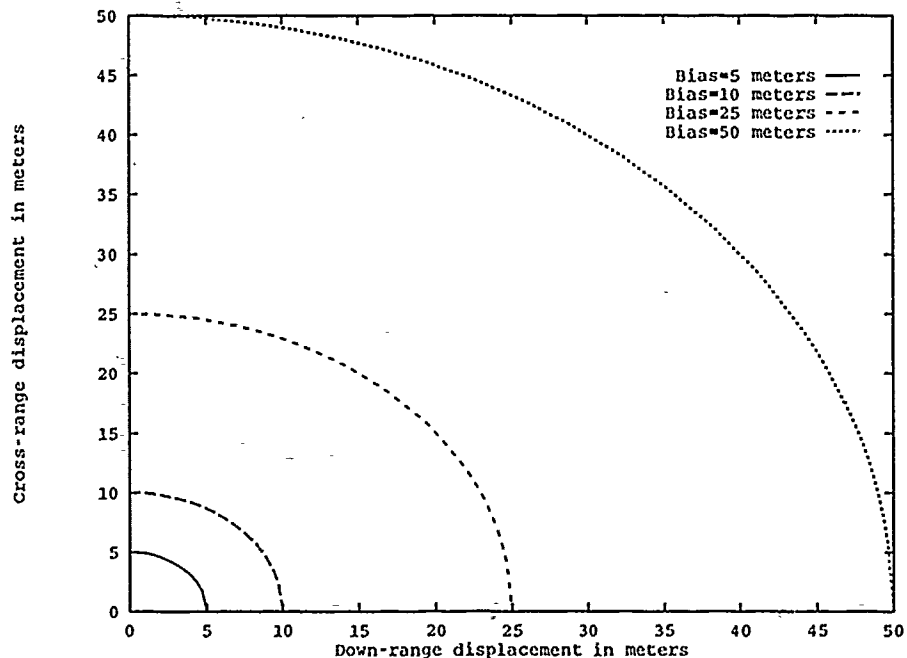


Figure 22. Bias-Limited Down- and Cross-range Displacement

The effect of flight-path angle error is difficult to show graphically. Appendix B contains derivation of typical influence coefficients for such errors, although they can be nearly eliminated by judicious choice of free-flight range. If the trajectory is designed to reach the maximum range, then the influence coefficient determining down-range displacement due to small errors in flight-path angle is *zero*, indicating *no displacement*. In fact, the characteristically small down-range error for an ICBM with a 3600 nautical mile, maximum range trajectory has been as little as *four feet* (1:303). To achieve minimal bias, it is assumed that the trajectory is designed to reach maximum range.

Figures 25 and 26 show cross-range displacement due to errors in burnout azimuth and lateral burnout point displacement. An azimuth error of 0.0005 degrees in combination with a lateral burnout point displacement of 5 meters is shown by these figures to result in relatively large re-entry point displacement, in this case between approximately 30 and 60 meters. Again, the burnout parameters determining cross-range errors must be precisely controlled if bias is to be held to a minimum.

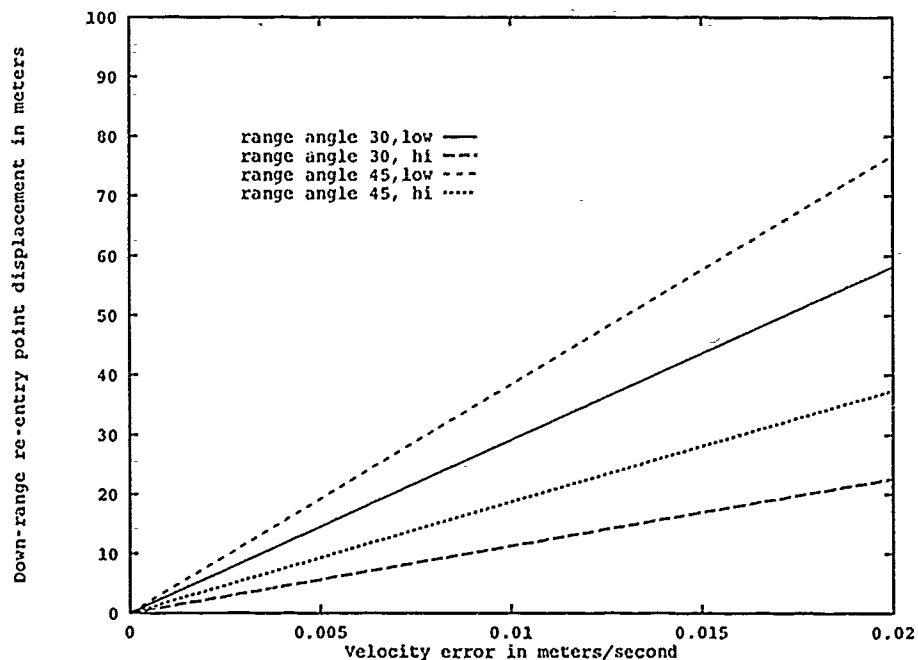


Figure 23. Down-range Displacement Due to Burnout Velocity Error

Finally, it should be stated that some of the above errors might have a “compensating” effect; an overshoot error in one parameter might cancel an undershoot error in another. Unless such effects can be guaranteed, however, the assumption should be made that they will not occur and treat the total error as an “upper bound.”

4.4 Responsiveness Axis Analysis

“Responsiveness” is defined herein to be a measure of how quickly a system can deliver ordnance to a target following an employment decision. Responsiveness of a Pegasus-based system must account for the status of both the launch vehicle and its carrier aircraft. It is also very mission-specific, since the carrier must fly to a drop point defined by the target and the range of the weapon. A top-down approach to estimating responsiveness is aimed at discovery of mission aspects that have the greatest influence on timeliness. This section describes typical phases in a potential Pegasus mission cycle and also gives insights into B-52 operations.

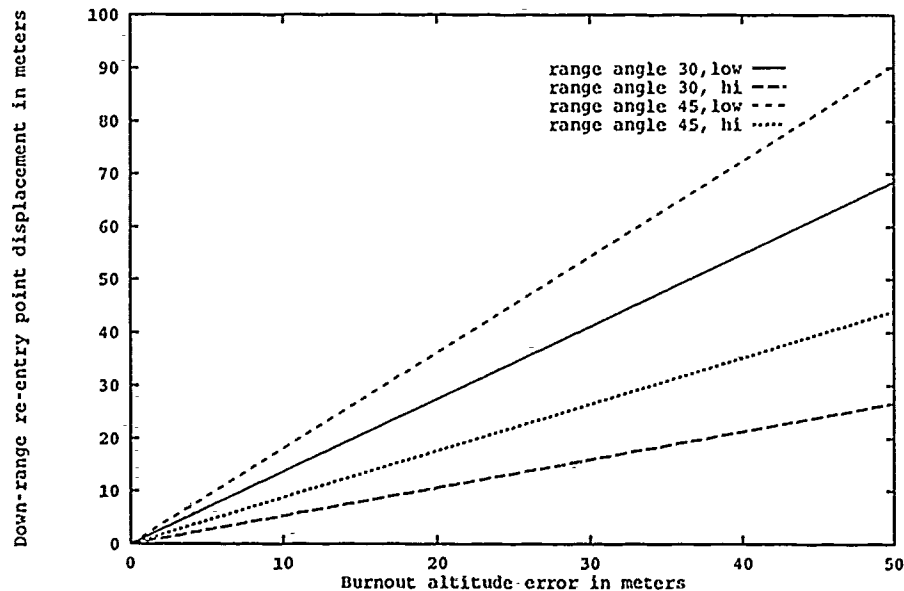


Figure 24. Down-range Displacement Due to Burnout Altitude Error

4.4.1 *Mission phases* A typical mission profile for the system under consideration consists of the following phases:

- *Mission planning.* This includes route planning by the flight crew and trajectory planning by a targeting branch.
- *Preflight.* This includes checkout and loading of the launch vehicle onto the aircraft, aircraft maintenance and fueling, and flight crew preflight activities.
- *Take-off/flight to the drop point.*
- *Pegasus flight to the re-entry point.* Determined by weapon range.

An additional phase occurs prior to those given above. The "intelligence phase" consists of target location from reconnaissance or other intelligence sources. Intelligence personnel must ensure that potential targets for the system are located to a great degree of accuracy so planners can determine the required drop point. "Opportunity targets" that appear on short notice must also be well defined positionally. The accuracy requirements for the Pegasus-based system are likely to preclude this type of target unless it can be expected to remain stationary for an extended period. This chapter cannot address all of the targeting considerations, but the timeline analysis

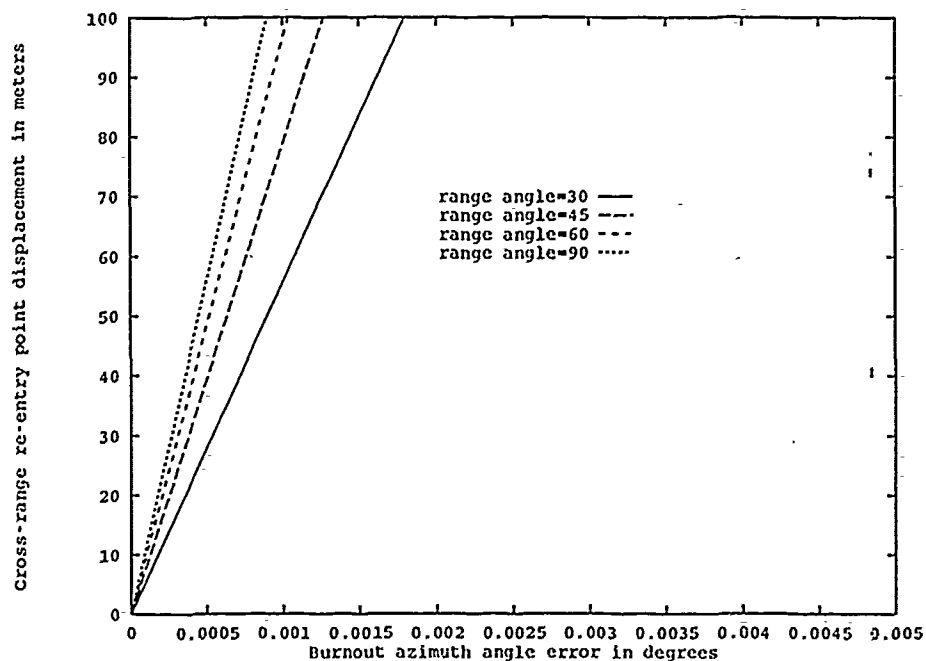


Figure 25. Cross-range Displacement Due to Burnout Azimuth Error

that follows can also “back into” an estimate of the minimum target stationary time that must be expected for it to be a candidate for Pegasus strikes.

4.4.2 USAF B-52 operations Pegasus was designed for launch from a B-52 aircraft, so this study assumes any USAF deployment would follow suit. Much is classified regarding bomber operations, but the performance of the aircraft is generally unclassified. Insight into how a Pegasus-type system would affect these operations may be obtained from those familiar with the aircraft. This study drew on the experience of Major Garrison Flemings, a B-52G aircraft commander with over 3000 hours flying time.

A Pegasus mission is likely to be fairly straightforward from an aircrew perspective. A given target requires that the rocket be dropped at a specific location, a specific time, and in a specific direction. The NASA crew flying the B-52 that dropped Pegasus on its first flight did so within 400 feet down-range, 1500 feet cross-range of the intended point (12:1). A drop error of this magnitude propagated to burnout could have resulted in a re-entry point displacement of 400 feet down-range (one-for-one error) and 600-1200 feet cross-range (from Figure 26). Errors in burnout

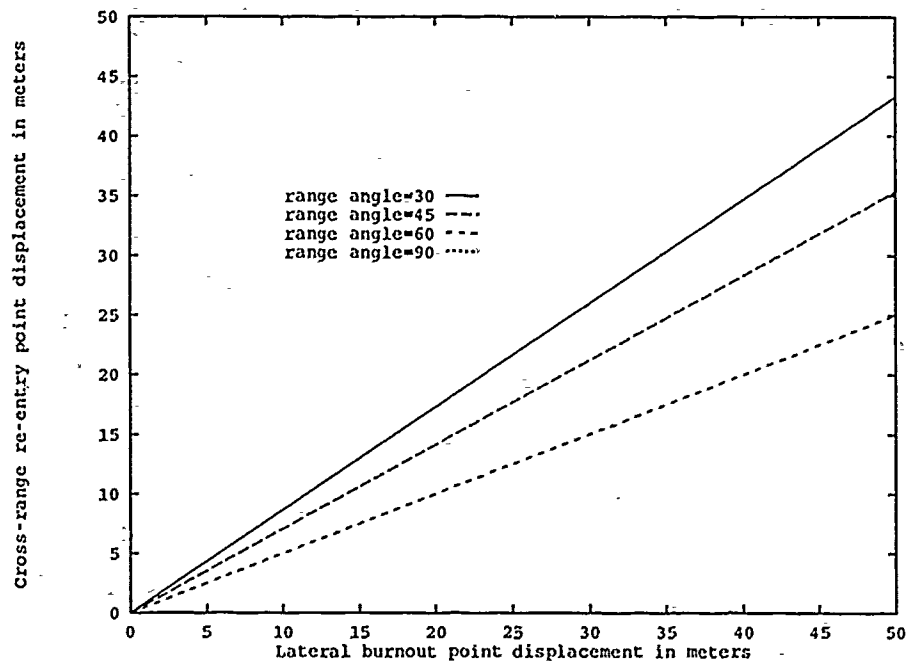


Figure 26. Cross-range Displacement Due to Lateral Burnout Point Displacement

conditions would have increased this displacement. Regular USAF aircrews practice their trade much more frequently, and Major Flemings indicates that much greater accuracy is expected and routinely achieved (3).

Detailed flight plans are not necessary for a crew prior to takeoff. A navigator will give a simple compass heading to fly toward the drop point, and will refine the directions once airborne. A refined heading will be given within 10 minutes, and detailed route instructions to the target soon thereafter (3). Drop time must be very accurate, but Major Flemings related that so long as requirements are not so severe as to require a straight-line flight to the drop point, a navigator is routinely capable of designing a series of U-shaped turns that result in the aircraft arriving very close to the planned drop time (3). The guidance system used by Pegasus would probably be required to correct for only minor errors in planned drop parameters.

The other factor of major importance to aircraft operations is maintenance. Major Flemings indicated that a particular aircraft receives approximately 8 hours of normal maintenance (called "Dash one time") before *every* mission. This figure might represent an unhurried pace, so it could possibly be reduced to as little as three

hours if the situation demands (3). Weapon loading would follow this maintenance, and then refueling. Time to load Pegasus is given below, but refueling time is on the order of one hour.

4.4.2.1 Mission Planning Phase. The section on B-52 operations indicates that the flight crew does not typically spend a great deal of time pre-planning their route. The time that is needed for mission planners to determine a particular profile depends on the degree of flexibility in the system. The range of the weapon is likely to be pre-determined and unchangeable, but the direction of attack will probably be variable. Expected error propagation and target characteristics determine direction of approach, which in turn dictates drop point location. The range from the B-52 base to the drop point determines if tanker support is needed. The unrefueled range of B-52 G/H models is mission-dependent, but is at least 3000-4000 nautical miles (15:9-10).

4.4.2.2 Preflight Phase. The time spent in this phase depends greatly on the alert status of the aircraft. An aircraft on alert is ready to go, weapons and fuel on board, awaiting the arrival of the flight crew. Aircraft not on alert must be prepared for a mission by maintenance personnel as described previously. Aircrew preflight activities take approximately 90 minutes to complete (3). The alert aircraft condition avoids all but aircrew preflight and gives a lower bound to the time for response. The unprepared aircraft gives the upper bound. Pegasus preparation time is also dependent on its alert status, total time varying between 2 and 10 hours (12:9-10). The time spent in this phase is dependent on the alert status of both the aircraft and the rocket vehicle and is broken out by activity in Table 5.

4.4.2.3 Take-off/Flight Phase. Time spent in this phase is determined by distance to the drop point. The specific time is mission specific, but bounds can be inferred. The first bound is governed by the minimum amount of time a B-52 takes to climb to the 41,000 foot-Pegasus drop altitude. Information contained in the B-52G performance manual can be used to determine this minimum time, which Major Flemings calculated to be approximately 15 minutes at normal rated thrust. The flight time to target may be estimated by dividing the distance by the B-52 "efficient operation" airspeed, 444 nautical miles per hour (3). Total flight time is range-dependent, but unrefueled maximum range provides another bound. The

Activity	System/Alert Status			
	B-52/Ready	B-52/Not ready	Pegasus/Ready	Pegasus/Not ready
Maintenance	0 hrs	4-8 hrs	N/A	N/A
Preflight	1.5 hrs	1.5 hrs	N/A	N/A
Checkout/fueling	0 hrs	1 hr	2 hrs	2-10 hrs
Loading	2 hrs	2 hrs	N/A	N/A
Total Prep Time	3.5 hrs	8.5-12.5 hrs	2 hrs	2-10 hrs
Total Integration Time	3.5 hrs	13.5 hrs		

Table 5. Preflight Phase Time Bounds

lowest value for maximum range is estimated by Major Flemings to be approximately 3800 nautical miles, giving a flight time of approximately 8.5 hours. A requirement for refueling would add several hours to this figure.

4.4.2.4 Pegasus Free-flight Time. Time spent in this phase is determined by the range to target. Assuming a symmetric trajectory, time of free flight is half the total unpowered time of flight. The following equation can be derived from Eq (17) by noting that $\nu = 180^\circ - \Psi/2$ (1:293):

$$\cos E = \frac{e - \cos \frac{\Psi}{2}}{1 - e \cos \frac{\Psi}{2}} \quad (57)$$

Vehicle free-flight time can thus be determined by

$$t_{ff} = 2\sqrt{\frac{a^3}{\mu}}(\pi - E + e \sin E). \quad (58)$$

The value for a , the semi-major axis, can be determined by solving Eq (19) for a given Q value. The trajectory eccentricity (e) can be found by the following equation (1:284):

$$e^2 = 1 + Q(Q - 2) \cos^2 \phi. \quad (59)$$

These equations can be used to calculate flight time for any set of burnout parameters. Table 7 of Appendix B indicates two typical parameter sets for Pegasus. The free-flight time for a 2-stage Pegasus might vary from approximately 9 minutes on a low trajectory, 3400 kilometer flight, to approximately 26 minutes for a maximum-range (6200 km) flight. A 3-stage Pegasus exhibits generally longer flight-times due to its greater velocity; a 3-stage flight to the 2-stage maximum range takes approximately 119 minutes.

4.4.3 Readiness Assessment With a premium on accuracy, it would be reasonable to expect Pegasus to follow a maximum range trajectory. For a 6200 kilometer Pegasus flight and 3000 kilometer B-52 flight to the drop point, the analysis in this section would yield a system response time to a mission tasking of between approximately 8.4 and 18.4 hours depending on alert status.

4.4.4 Responsiveness and Reliability The timeline discussion in this section is based on all components functioning as planned. The values derived are therefore lower bounds on total time but are valuable for seeing the contribution of individual phases. The mission might be at best delayed and at worst cancelled if either the aircraft or Pegasus malfunctions. Extensive analysis of reliability issues is beyond the scope of this research.

4.5 "Backing In": a GPRC Example

Chapter 1 alludes to AFSPACECOM having already been presented with a potential Pegasus-based system called "Global Precision Response Capability", or GPRC. The developers of the system describe it as having "surgical precision" and "less than 4 hour response time" (16:5). The analysis approach presented in this thesis can be used to "back into" the assumptions that must be made for these claims to be realizable.

4.5.1 GPRC Responsiveness Major Flemings' description of B-52 operations as summarized in Table 6 reveals that the only way for GPRC to achieve a responsiveness of less than 4 hours from call-up is for the system to be on alert status, indicating at least a 1.5 hour pre-flight time assuming the weapon is already loaded or a 3.5 hour preparation time if it is not. The B-52 carrier aircraft takes at least 15 minutes to reach the 41,000 foot drop altitude. Assuming that the Pegasus drop

point is located immediately upon reaching this altitude and that the B-52 is flying at exactly the proper speed and direction, between 1/4 and 2 1/4 hours remain out of the original four hours for the weapon to fly to its target. This should enable flight to most any reasonable range. Four hour responsiveness is theoretically possible although it is optimistic. A Pegasus-based weapon system held on ready standby with the weapon loaded on the aircraft and the aircraft ready to roll might be capable of a 4-hour response, so long as the launch point is close to the airfield. Any other condition casts doubt on this claim.

4.5.2 GPRC Precision The definition of "surgical precision" is not given in the unclassified version of GPRC. Inferences may be made, however, based on the warhead design. The payload of GPRC consists of a cluster of 36 kinetic-energy (KE) penetrators that are designed to be released at the same time and which then deploy into a pre-set pattern centered on the target (16:28). The fact that KE warheads are used indicates that a target must be struck directly or very nearly so by one or more of the weapons in order to be damaged. The lethal area of an individual KE weapon is likely to be very small, dictating a correspondingly small CEP. As an example, if the CEP is on the order of 40 meters and a reasonable PD (e.g., 0.8) is required, then Figure 18 indicates that the target must have a radius of at least approximately 75 meters. This is a relatively large area, so the types of targets are likely to be limited. It is worth repeating that CEP defines a radius in which *half* of the shots at a given target are expected to fall, so a single-warhead design is likely unacceptable. Assuming a 40 meter CEP necessitates a maximum bias of approximately 30 meters (Figure 19). Table 6 shows the maximum error in each parameter, assuming it alone contributes to the 30 meter bias. Important to note in the table are the extremely small allowable errors in the velocity vector magnitude (v_{bo}) and direction (ϕ_{bo} and azimuth) to achieve this level of performance. Either Pegasus avionics has to be capable of a very high degree of precision and control, or the re-entry system "bus" has to be capable of correcting the trajectory after separation from the launch vehicle.

The 36 warhead design of GPRC effectively increases the overall lethal area of the system. Each individual KE penetrator is claimed to be capable of up to 150 meters of displacement for the purpose of pattern development (16:28). Further analysis of alternative patterns could possibly relax the stringent requirements on burnout conditions to some degree.

<i>Parameter</i>	<i>Maximum Error</i>
r_{bo}	17-55 m ¹
v_{bo}	0.0075-0.03 m/sec ²
ϕ_{bo}	³
in-plane burnout point displacement	30 m
azimuth	0.0005-0.0003 ⁴
lateral burnout point displacement	34-1700 m ⁴

¹: From Figure 25 (Representative values)

²: From Figure 24 (Representative values)

³: Will be nearly zero if max range trajectory

⁴: 30° – 89° range angle

Table 6. Maximum Allowable Parameter Errors: 30 Meter Bias

The definition of “surgical” must be explicit with regard to its assumptions. A small CEP requires the bias to be small. Limiting the bias implies small down-range and cross-range error tolerances, which in turn necessitate small parameter error tolerances. Table 6 shows the maximum errors in each parameter if bias is to be held to 30 meters, but a GPRC-like system would probably have to have at most a 10 meter displacement due to the cumulative effects of *all* parameters.

Chapter 3 presented the rocket theory that describes how the specific impulse of a solid rocket motor (as employed by Pegasus) affects system performance. Constraining burnout velocity to a maximum error of 0.01 meter/sec implies that specific impulse must be similarly controlled. Pegasus stage 2 effective specific impulse is given at 290.2 seconds, so allowing this to vary only 0.01 seconds indicates a controllability of the parameter to within 0.003%. Similarly, if burnout altitude must be limited to a 10 meter error, then burn time must be controlled to within approximately 0.002 seconds, or to within 0.001% of a typical 2 stage Pegasus burn time. Such control implies tight restrictions on propellant weight, since a solid rocket burns until all propellant is consumed. Whether GPRC can meet these constraints, or compensate for not doing so through re-entry bus design, is a matter for engineers to decide. It is unlikely that such a system would be capable of dropping a warhead down an air shaft. It might be capable of limiting “collateral damage”, but this

ability may be attributed as much to a small individual warhead lethal radius as to any inherent system accuracy.

4.6 Chapter Summary

The mission capabilities of a ballistic-trajectoryed space strike system are defined by its ability to respond quickly to the discovery of a threat, and deliver a payload over a specified range to within an acceptably close vicinity of its target. Using a Pegasus-based system to fulfill this mission concept bounds the potential requirement space by the specific capabilities of the system.

Responsiveness was shown to be highly dependent on the alert status of the integrated B-52/Pegasus system, with secondary dependence on distance to the drop point and target range.

Specifying a certain minimum range capability dictates a set of burnout conditions that will attain it. These conditions in turn determine the system's design requirements. Two of the three factors that determine range—burnout velocity (v_{bo}) and burnout altitude (r_{bo})—are primarily functions of the Pegasus launch system and thus a certain minimum range capability sets the requirements Pegasus needs to attain. The third factor—burnout flight-path angle (ϕ_{bo})—is a requirement for the re-entry vehicle. Steeper values of ϕ_{bo} are typically more difficult to design for than shallower values although this thesis illustrates the fact that a specific range requirement may be achieved by several different ϕ_{bo} settings. The accompanying top-down PD axis analysis, however, shows that shallower angles are not conducive to highly accurate delivery.

Defining a minimum PD that must be attained determines the acceptable target size/weapon CEP combinations that will achieve the given level. Target size limits the type of target that may be considered as well. Specifying CEP implies a set of maximum values for down-range and cross-range bias. This (systematic) bias places limits on the available magnitude of down-range and cross-range error. Finally, it was shown that total down-range and cross-range bias errors are the result of parameter error, and even small errors in parameter values lead to relatively large down-range and cross-range displacements.

V. Conclusions

Conclusions drawn from a top-down analysis do not *answer* the fundamental question. Rather, they provide the individual who does make the decision a means of "backing into" the range of assumptions that must be made for a particular decision to be correct. The analyst establishes the performance bounds of the fundamental decision space, but the decision maker must be the one who decides if these describe an acceptable set of capabilities. A positive decision based on a top-down analysis of the problem tells the executive *why* his decision is feasible, and it tells the engineers *what* to concentrate their efforts on. A negative decision is the result of failure to perform in one or more critical areas, and everyone from engineer through analyst to executive understands why the decision was made.

The top-down approach is ideal for addressing a variety of feasibility-type issues in the Air Force. The products of the approach provide a "bridge" between engineers and policy makers that is grounded in technical issues but understandable to those less technically oriented. Policy makers decide how a system is to be used but seldom are aware of the current technological "state of the art". Engineers know the hardware but often are not privy to the full mission of the systems they design. A top-down analysis, aimed at establishing fundamental trade-off relationships, fills the gap. Policy makers can read the study and understand the drivers, thereby bounding their concept of potential missions. Engineers can see how the individual components affect the final result and can concentrate on the technical feasibility issues. The analyst who performs the study understands the issues involved and serves as a channel from top to bottom, minimizing the intentions vs. capabilities disconnect.

The top-down approach applied to the Pegasus system has shed light on the important issues driving any decision to develop it further. The system is potentially capable of reasonable accuracy in absolute terms, but whether it can compete with truly "surgical" munitions of the type employed in Desert Storm depends on the mission it is tasked to perform. A Pegasus-based strike system's real utility might be in the "show of force" arena, where it could be used to demonstrate US ability to strike high value targets without any possibility of defense. If it is determined that Pegasus cannot achieve the accuracy requirements set out for it, then it must either

be redesigned or the RVs it employs must be improved by the inclusion of "smart" technology. Active, "man-in-the-loop" guidance will probably not be feasible due to high re-entry speeds and correspondingly short target acquisition time. An RV incorporating limited maneuverability with simple target pattern recognition could, however, significantly increase system effectiveness.

There are many other issues requiring study before a space strike weapon of any kind could be deployed including such "soft" issues as international legality and the political aspects of conventional attack from space. This thesis has attempted to shed some light on the engineering and implementation concerns that need to be addressed in order to answer the question "*Can* such a system be developed?" These other issues deal with the potentially more delicate, yet no less fundamental question "*Should* we deploy this type of system?" These issues must be resolved before pursuit of the concept can be performed.

Appendix A. Pegasus Performance Boundaries

The specific parameter ranges achievable by the Pegasus launch system bound the potential capabilities of a strike system derived from it. This section sets these limits and is based on the most recent published Pegasus design characteristics (13).

Figure 27 shows performance characteristics for the first three solid rocket-propelled stages of the Pegasus launch vehicle.

Parameter	Units	Stage 1 Motor	Stage 2 Motor	Stage 3 Motor
	Metric			
Overall Length	cm	888.0	265.7	133.9
Diameter	cm	127.5	127.5	96.5
Inert Weight	kg	1,257 (1)	343	126
Propellant Weight (2)	kg	12,160	3,024	771
Total Vacuum Impulse (3)	kN-sec	35,108.1	8,666.5	2,183.1
Max. Case Pressure	kPa	7,378	6,764	4,585
Average Pressure	kPa	5,840	5,826	3,785
Burn Time (3) (4)	sec	72.4	73.3	68.4
Max. Vacuum Thrust (3)	kN	580.46	138.64	35.81
Vacuum Specific Impulse (5)	N-sec/kg	2,888	2,867	2,834
Vacuum Specific Impulse Eff.	N-sec/kg	2,874	2,847	2,811
Expended Inerts	kg	62	21	6
Initial Expansion Ratio	—	40:1	65:1	60:1
Initial Throat Diameter	cm	22.45	10.67	6.81
Exit Diameter	cm	142.0	86.1	52.6
TVC Deflection	deg	na	±3	±3
Notes: (1) Including Wing Saddle, Truss and Associated Fasteners (2) Includes Igniter Propellants (3) At 21° C (4) To 207 KPa (5) Delivered (Includes Expended Inerts)				

Figure 27. Pegasus Motor Characteristics (reproduced from (13:2-5))

Figure 28 gives upper bounds on possible velocities for Pegasus, based on the "ideal velocity gain" equation (Eq (50)) and the weight values given in Figure 27. The values given are upper bounds because they do not include aerodynamic effects, velocity loss during staging, etc. The maximum altitude at which burnout may occur is a function of vehicle velocity. For a rocket launched vertically, maximum altitude

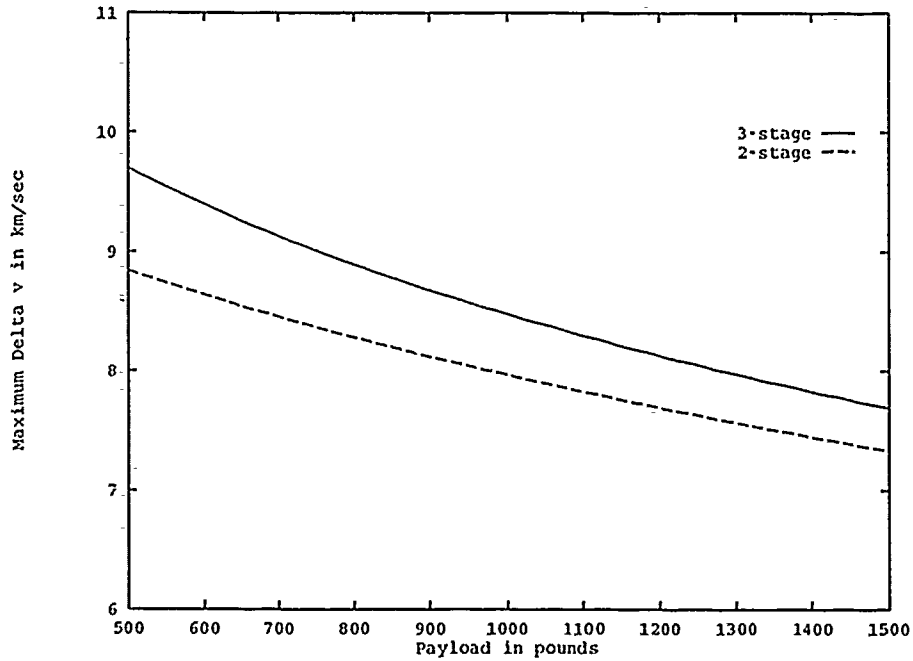


Figure 28. Pegasus Theoretical Velocity vs. Payload

may be estimated by the basic physics equation

$$h = h_o + v_o t - \frac{1}{2} a t^2 \quad (60)$$

where h_o is the initial altitude (12.5km in the case of Pegasus), v_o is the initial velocity, t the time of flight, and a the gravitational acceleration. Pegasus is launched horizontally and so the distance travelled down-range during its initial flight takes away from the maximum possible altitude. Constraints imposed by the maximum initial climbing angle further limit altitude; higher angles may allow greater altitude by permitting a steeper climb during powered flight. Shallow angles could entail a more gradual climb and thus a lower maximum altitude. Figure 29 shows theoretical maximum altitudes for a range of velocity/climb angle combinations, using the 2-stage Pegasus burn time given in Figure 27 and assuming $a = 9.8m/sec^2$. The figure assumes drag-free, straight-line flight at the indicated angle. It also assumes continuous operation at constant velocity. The values therefore indicate upper bounds on theoretical capability.

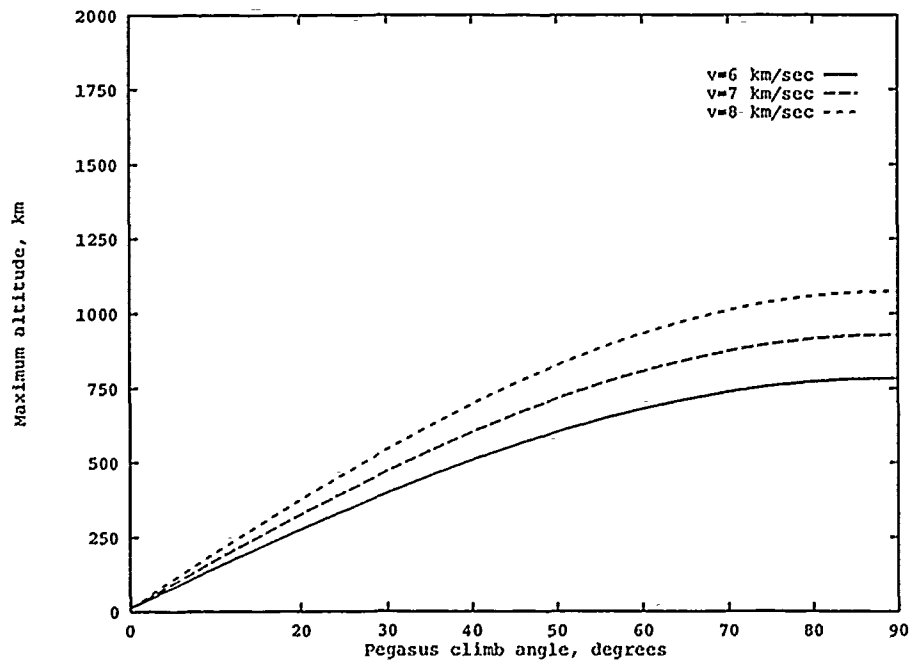


Figure 29. Theoretical 2-stage Pegasus Maximum Burnout Altitude

Bounding of burnout flight-path angle (ϕ_{bo}) values is difficult since it depends on the specific re-entry vehicle (RV) design. Consequently, any reasonable value may initially be assumed pending engineering analysis of specific designs.

Appendix B. Burnout Parameter Interactions

This section describes the derivation of influence coefficients for the burnout parameters of altitude (r), velocity (v), and flight-path angle (ϕ), and how these lead to re-entry location displacement.

B.1 Re-entry Location Displacement

Total re-entry point location displacement can be expressed in terms of a down-range and a cross-range component. The down-range component arises as the result of errors in burnout altitude (r_{bo}), burnout velocity (v_{bo}), and burnout flight-path angle (ϕ_{bo}). The cross-range component is generated by either a physical displacement of the burnout point or an error in the *direction* of the burnout velocity vector called launch azimuth. This section evaluates down-range errors with respect to each burnout parameter. Then, cross-range errors are similarly analyzed.

Once a Q value is established from Eq (18), Figure 30 can be used to determine the theoretical free-flight range, expressed as a distance for ease of understanding. This figure is generated by solving the free-flight range equation (Eq (24)) for a set of flight-path angles and over the specified Q -value range.

The requirement for flight-path angle is typically set in advance (eg.: for GPRC, $\phi = 40^\circ$) so it is also useful to determine ranges for specific ϕ values. Figures 30 and 31 contain similar information except that in the latter, range is listed as a function of flight-path angle. The curves in the figure are derived from solving the flight-path angle equation (Eq (33)).

Figure 31 illustrates how the flight-path angle required to attain a given range increases rapidly until the maximum range point is reached, and then decreases more gradually. The significance of this is subsequently discussed in the section on parameter error sensitivity, where it is seen that the low trajectory (smaller flight-path angle) for a given range is more sensitive to parameter errors than the high trajectory. The lines on this figure are *not* symmetric, so unlisted combinations of parameters must be individually plotted; interpolation between listed values is not recommended.

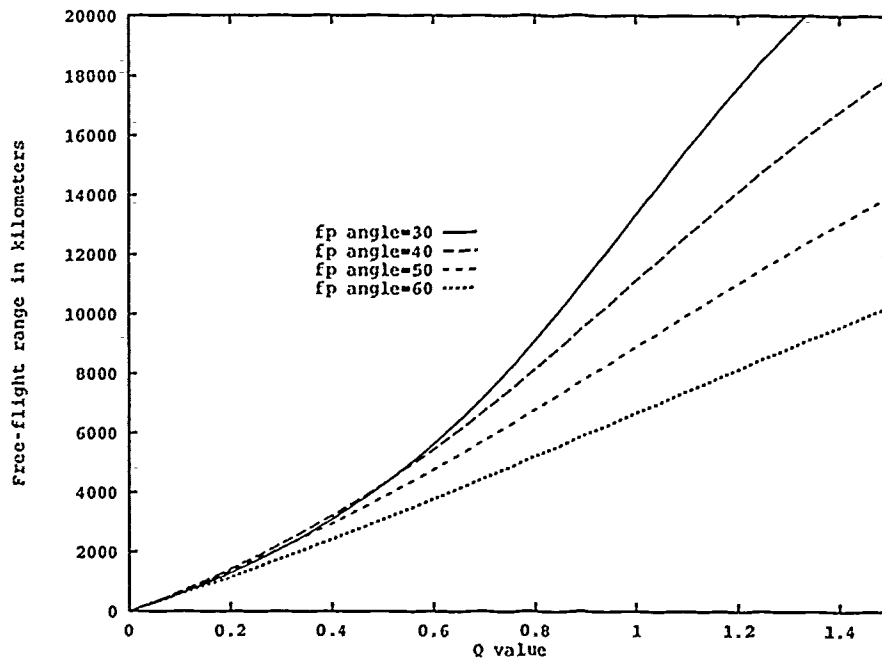


Figure 30. Free-flight Range (Ψ) vs. Q -value

B.1.1 Down-range Displacement The effect of individual parameter error on down-range displacement is the product of the magnitude of the deviation and the partial derivative of the free-flight range equation (Eq (24)) with respect to that parameter. Chapter three contains the derivation of these partials for each burnout parameter. Error effect is dependent on particular combinations of parameter values, and generalization is not usually possible (e.g., the values of ϕ possible to reach $\Psi = 30^\circ$ varies for different Q values). Table 7 lists the "planned" burnout conditions used for illustration. The 3-stage example is representative of the theoretical "upper performance bounds" described in Appendix A, and the 2-stage values are taken from an example ballistic trajectory described in the *Pegasus Payload User's Guide* (13:9-2).

The next graphs show the effects of errors in burnout velocity for two cases. The first specifies the range, but allows a choice between the low and the high trajectories. The second specifies the flight-path angle but allows the range to vary. The charts compare the effects of a low Q value (represented by the Table 7 2-stage conditions) and a higher Q value (the 3 stage example). Errors are expressed as a

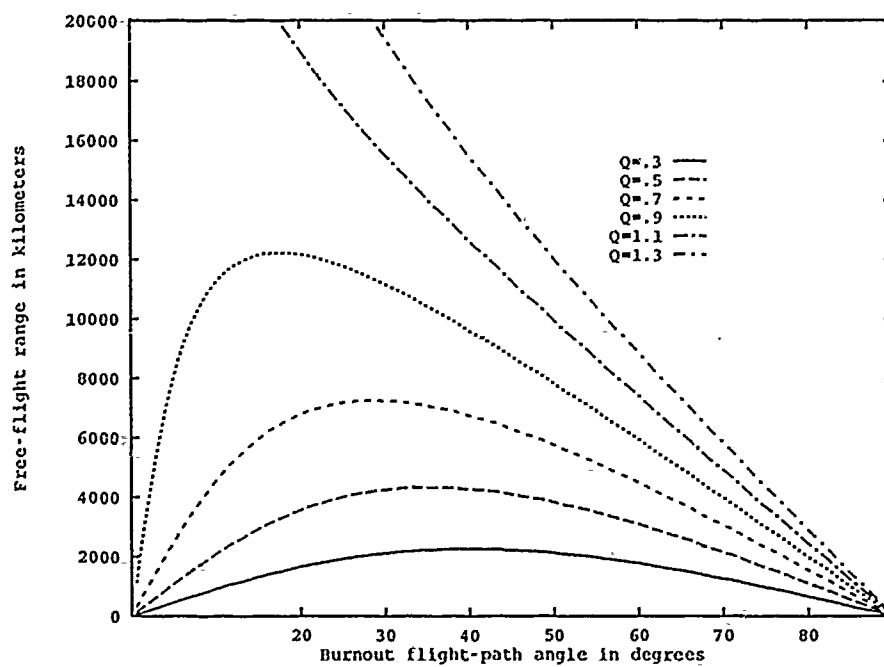


Figure 31. Free-flight Range (Ψ) vs. Flight-path Angle (ϕ)

Velocity	Altitude	Q value	Description
6.3 km/s	300 km	0.665	2-stage, 850 lb
8.3 km/s	600 km	1.206	3-stage, 1000 lb

Table 7. Typical Pegasus Parameter Combinations

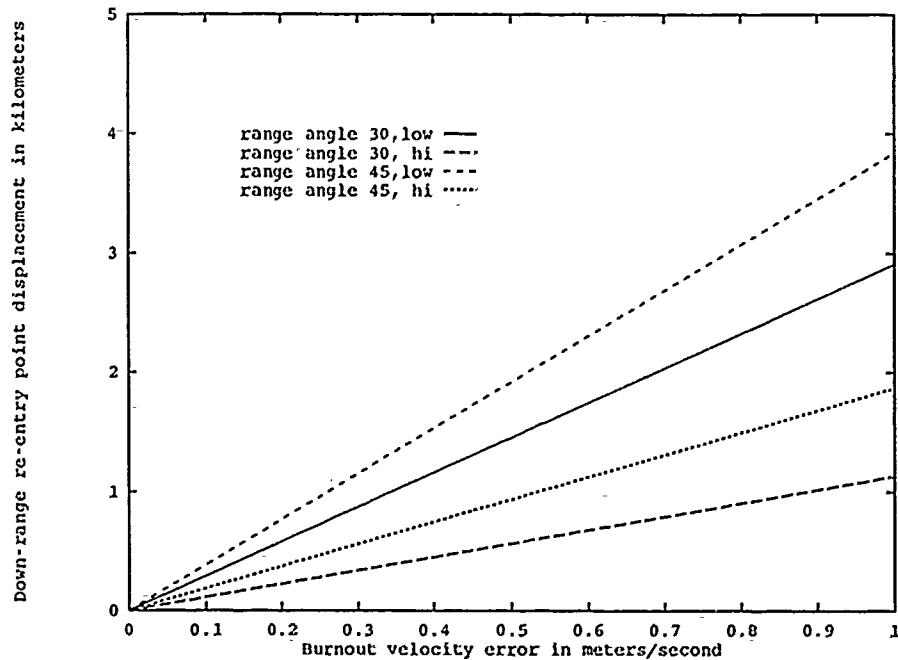


Figure 32. Typical 2-stage Velocity Error Effects, High vs. Low Trajectories

positive number, which would represent higher than planned velocity, which results in re-entry farther than planned ("overshoot"). Negative values correspond to lower than planned velocity and would result in "undershoot". The effects of a negative velocity error propagate in exactly the same manner as the positive values listed.

Figure 32 is generated by solving the flight-path angle equation (Eq (33)) for the indicated range angles using the 2-stage parameter values listed in Table 7. The values for downrange displacement are determined by solving Eq (40) for the given parameter sets. Three-stage values are not used since $Q > 1$ leading to only a high trajectory for any given range. Several important concepts are illustrated by this figure. First, the high trajectory is less sensitive than the low to errors in burnout velocity. A deviation in burnout velocity of 1.0 meter/second results in a down-range deviation of approximately 2900 meters for a 30° range angle on the low trajectory, but only a 1100 meters deviation following the high trajectory. The same relationship can be seen in the 45° range angle case. Next, longer ranges show greater sensitivity to velocity error. Even on the less-sensitive high trajectory, a 1.0 meter/second error in velocity imparts a down-range displacement of 1800 meters, as

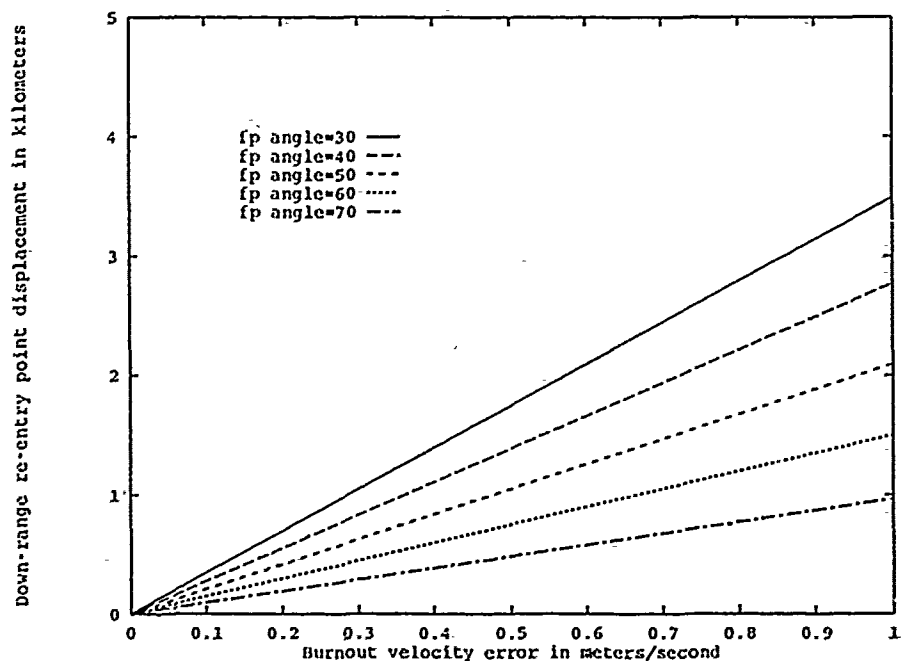


Figure 33. Typical 2-stage Velocity Error Effects, Fixed Flight-path Angle

opposed to 1100 meters for the 30° case. Also, relatively small velocity errors produce large down-range errors. One meter/second out of a planned 6300 meters/second (0.01%) results in a miss of over 1000 meters. Finally, the chart may be used to determine the velocity error "influence coefficient". This number is the down-range displacement corresponding to a velocity error of 1.0 meter/second. Since the effect of velocity error for a specific set of conditions is linear and proportional, the down-range displacement for any error value may be found by simply multiplying the error by the influence coefficient. This is an important concept that is used in analysis of altitude and flight-path angle errors. Figures 33 and 34 show that steeper angles produce smaller errors, with the total down-range displacement proportional to the velocity deviation. Also, a higher Q value induces more displacement than a lower Q value for a similar velocity error. A deviation of 1.0 meter/second with a flight-path angle of 30° results in down-range displacement of approximately 5700 meters for the 3-stage example, but only 3500 meters for the 2-stage example.

Down-range displacement of the planned re-entry point due to error in burnout height is now discussed. The values of Ψ and ϕ_{bo} used to generate the plots are the

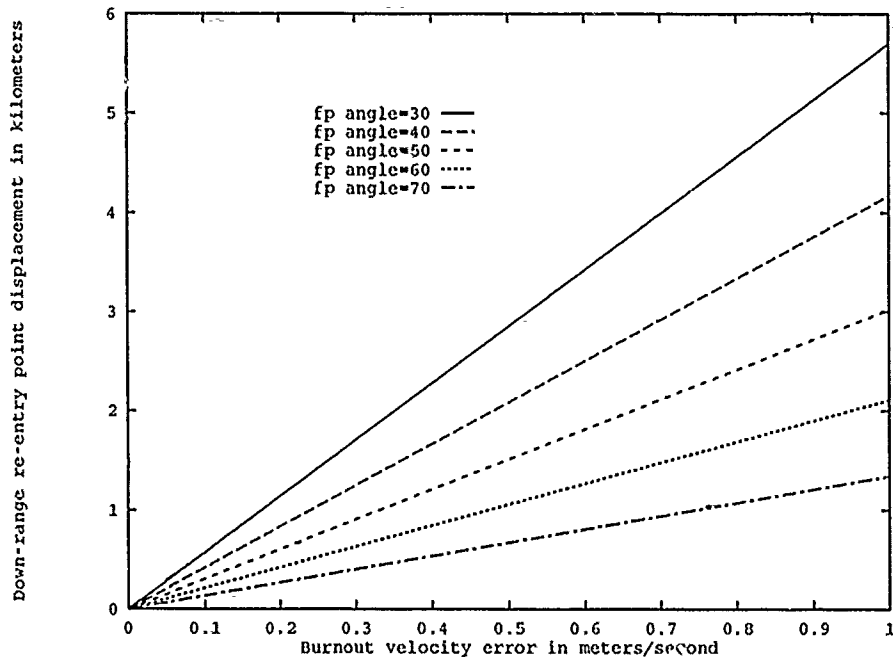


Figure 34. Typical 3-stage Velocity Error Effects, Fixed Flight-path Angle

same as those used in the velocity error analysis, and the nominal burnout altitudes are those given in Table 7. The errors are found by solving Eq (38) for the given range of Q , z_{bo} , Ψ , and ϕ_{bo} values. Figure 35 shows that high trajectories are less sensitive to errors in burnout altitude than low trajectories for a given range angle, with longer ranges exhibiting greater displacements. The magnitude of down-range displacement is also seen to be generally less for altitude errors than for velocity errors. Figure 36 curves are derived with using a smaller Q value than that used for Figure 37 (both given in Table 7). The relative effect of burnout altitude error is greater for higher Q values (Figure 37) than for lower values (Figure 36). In addition, down-range displacement is less for larger flight-path angles regardless of the particular Q value. Error propagation is the same as that for velocity errors: higher than planned values result in overshoot, lower than planned result in undershoot.

Equation (47) seems to indicate that down-range errors due to incorrect burnout flight-path angle (ϕ_{bo}) depend only on the planned values of range (Ψ) and ϕ_{bo} , but, this is misleading. The derivation of the equation (see Chapter 3) initially contained

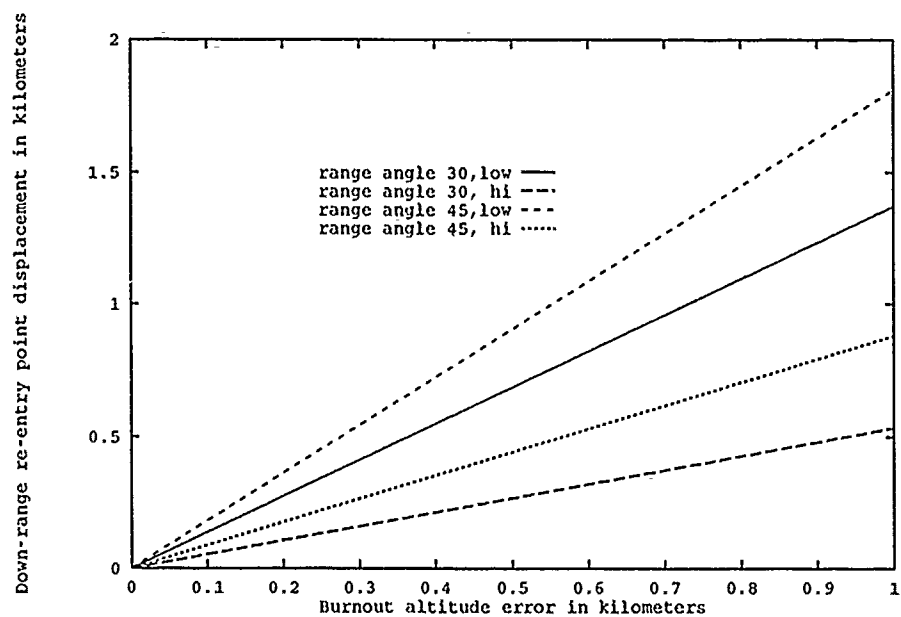


Figure 35. Typical Altitude Error Effects, High vs. Low Trajectories

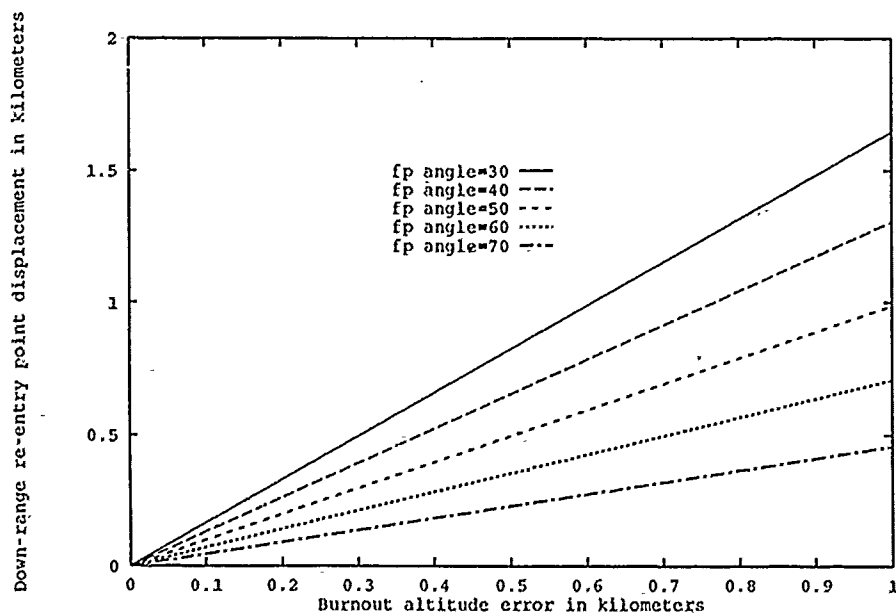


Figure 36. Typical 2-stage Altitude Error Effects, Fixed Flight-path Angle

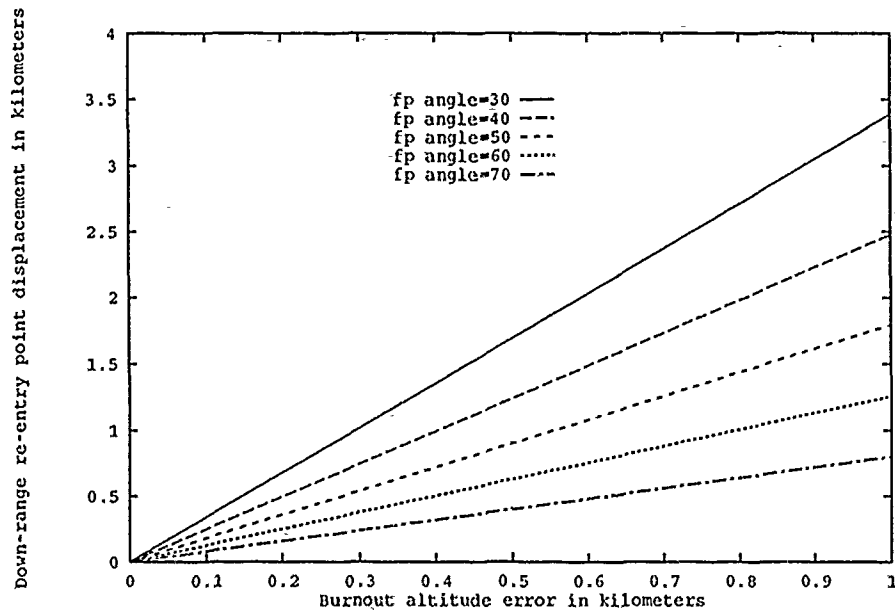


Figure 37. Typical 3-stage Altitude Error Effects, Fixed Flight-path Angle

a Q term, but it was eliminated in the simplification process. Analysis of specific ϕ_{bo} error effects must also be based on specific Q values.

Figure 38 reproduces two of the curves from Figure 31. Figure 39 shows that a typical Q value less than one results in potential range angle values that follow a generally parabolic curve with the apex corresponding to the maximum range. The partial derivative of Ψ with respect to ϕ_{bo} (which determines flight-path angle error effect) is the slope of the curve at any point. The effect on re-entry point displacement for any given combination of Ψ and ϕ may be estimated by referring to Figure 38 and Eq (42). The figure shows that for $Q < 1$, the value of the slope of the curve is typically greater for low trajectories (steeper slope) than for high trajectories. The positive slope for low trajectories indicates that a positive error (greater than planned flight-path angle) results in overshoot, while a negative value results in undershoot. The slope for high trajectories is negative, causing exactly the opposite relative error propagation. The point of maximum range separates the low from the high trajectories, and the slope at this point is zero. This last fact merits repetition: *for the maximum range case, there is no down-range displacement for "small" errors in flight-path angle* (1:302). For $Q > 1$, there is no low trajectory and no maximum range, so only the high trajectory case applies. To convert to

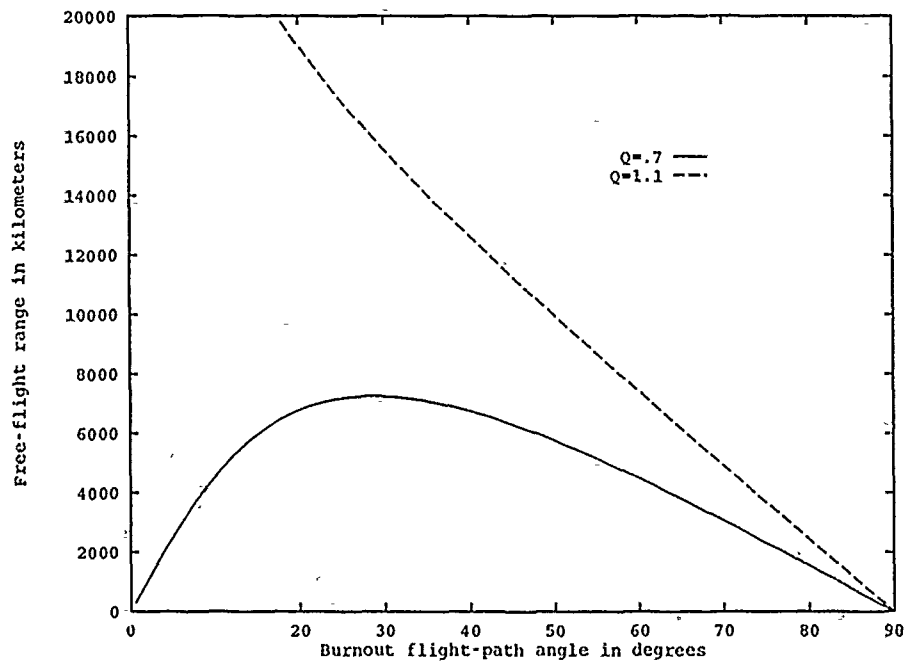


Figure 38. Selected Range-angle/Flight-path Angle Curves

distance, multiply the slope of the appropriate range/flight-path angle curve at the desired point by 111.319 kilometers/degree. To determine the resulting displacement magnitude, multiply this number by the flight-path angle error. Tables 8 and 9 give typical values of slope \times conversion factor for selected-range/flight-path angle pairs.

The tables exemplify the magnitude of down-range error possibilities for even small errors in flight-path angles. Proper design can greatly reduce these errors if an appropriate Q value can be chosen so that the re-entry flight-path angle occurs at the maximum range.

$\Psi = 30^\circ$		$\Psi = 40^\circ$		$\Psi = 56.75^\circ$ (max range)
$\phi = 66.8^\circ$ (hi)	$\phi = 8.15^\circ$ (lo)	$\phi = 58.3^\circ$ (hi)	$\phi = 11.6^\circ$ (lo)	$\phi = 30.06^\circ$
-135.8*	350.8*	-123.7*	229.9*	0
*:unit= kilometers/degree error				

Table 8. Typical 2-Stage Flight-path Angle (ϕ) Error Displacement Effects

$\Psi = 30^\circ$	$\Psi = 40^\circ$	$\Psi = 56.75^\circ$	$\Psi = 127.58^\circ$
$\phi = 77.6^\circ$	$\phi = 73.5^\circ$	$\phi = 65.5^\circ$	$\phi = 40^\circ$
-270.6*	-272.4*	-277.5*	-327.3*
*:units=kilometers/degree error			

Table 9. Typical 3-stage Flight-path Angle (ϕ) Error Displacement Effects

B.1.2 Cross-range Displacement The effects of incorrect launch azimuth and lateral displacement of the burnout point on re-entry point displacement may be shown completely and without assuming particular burnout parameter values. The first graph, Figure 39, shows the effect of incorrect launch azimuth, and is derived by solving Eq (47) for a set of typical range angles (Ψ values). The second graph, Figure 40, illustrates the case of lateral displacement at burnout, and is based on solving Eq (45) for the same range of Ψ . Figure 39 shows that the magnitude of re-entry error increases with increasing range angle (Ψ), and is a maximum for $\Psi = 90^\circ$. The effect then decreases symmetrically with the previous increase until $\Psi = 180^\circ$, where the error is theoretically 0 regardless of the launch azimuth. Figure 39 also shows the large potential effect of azimuth errors on cross-range location. Errors left of planned azimuths result in cross-range displacement to the left, and errors to the right of planned result in displacement to the right.

Figure 40 shows that increasing the trajectory range exhibits *less* sensitivity to lateral displacement of burnout, until $\Psi = 90^\circ$, at which point the error is zero. Cross-range error is symmetric about the 90° point, reaching a theoretical maximum at $\Psi = 180^\circ$. Figure 40 also shows that lateral burnout point displacement is far less influential on cross-range error than azimuth error. Displacement left (right) of the intended point results in left (right) re-entry displacement for ranges less than 90° . For trajectories of range greater than 90° , displacement left (right) of intended produce re-entry displacement to the right (left).

B.2 Influence Coefficient Determination

Influence coefficients for down-range error factors are given in Table 10. The values given for typical coefficient ranges are determined from the preceding analysis. Specific values are situation-dependent, but those in the table can be considered representative performance bounds.

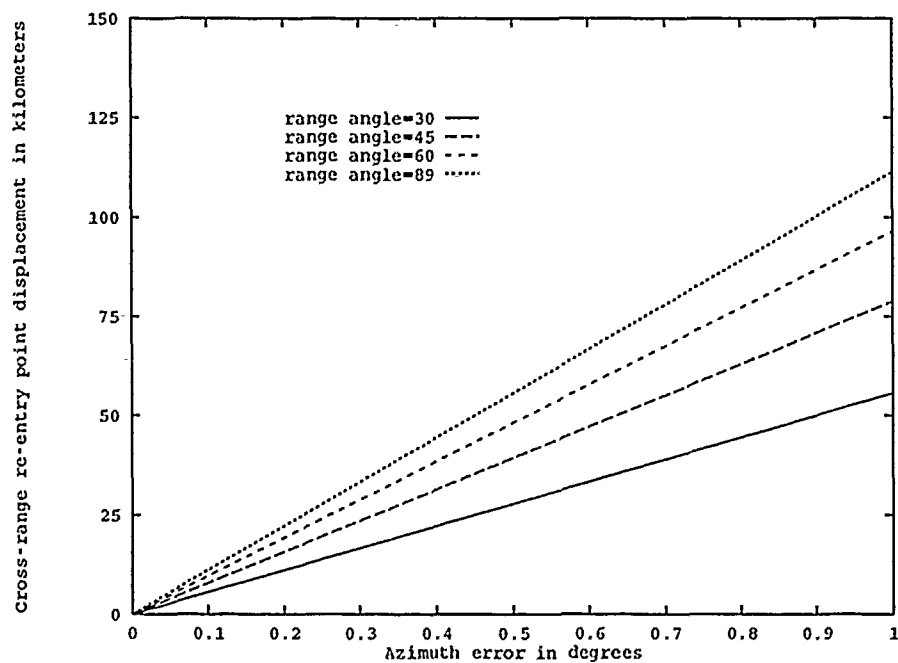


Figure 39. Cross-range Errors Due to Burnout Azimuth Error

<i>Parameter name</i>	<i>Influence coeff. "units"</i>	<i>Down-range displacement per "unit" of error</i>
altitude (r)	1 km/(km error)	1-3 km
velocity (v)	1 km/(m/s error)	1-5 km
flight-path angle (ϕ)	1 km/(degree error)	100-300 km

Table 10. Down-Range Displacement Influence Coefficients

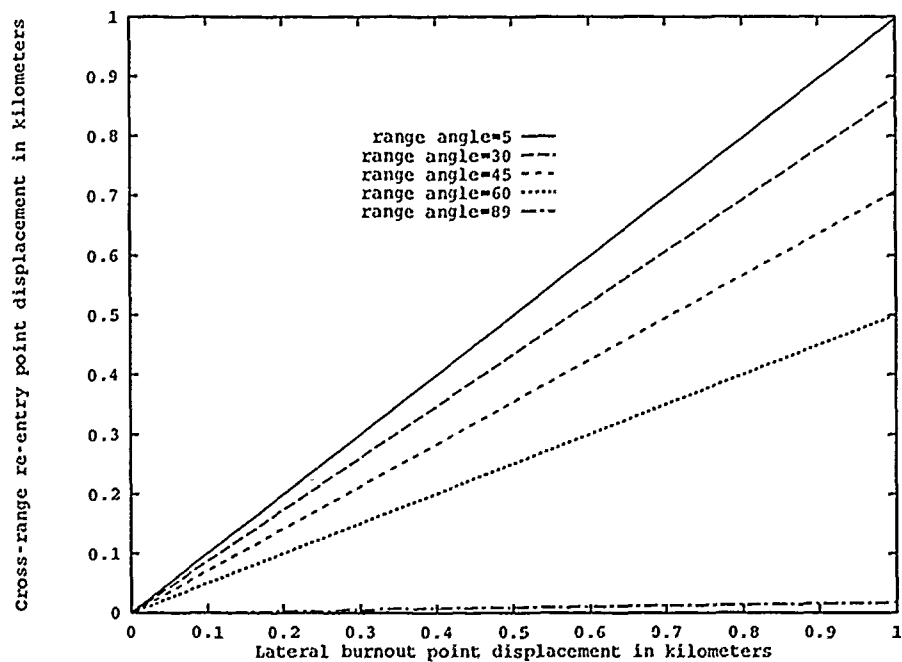


Figure 40. Cross-range Errors Due to Lateral Burnout Point Displacement

Influence coefficients for cross-range displacement may be determined as well. Examination of Figure 39 shows that the typical influence coefficient range is between 60 and 120 kilometers cross-range displacement per degree error in burnout azimuth. The effect of lateral burnout point displacement is much smaller, yielding a re-entry location displacement of 0.5-0.9 kilometers per kilometer error.

Appendix C. *Ancillary Effects*

Determination of fundamental relationships regarding accuracy of a ballistic vehicle can be made under the assumption of ideal conditions. High accuracy, however, requires that real physical phenomena be as accurately modelled as possible to reduce any systematic error effects. This section describes some of the effects of earth oblateness, atmospheric drag, and earth rotation.

C.1 Earth Oblateness Effects

Gravity exerts by far the greatest influence on the free-flight and re-entry phases of a ballistic trajectory. The theoretical impact point in a central gravity field (such as that of a perfectly spherical earth) may in fact be displaced significantly by the actual, non-spherical earth. With a burnout-target longitude difference of 75° , and under a given set of velocity and flight-path angles, the impact point can be displaced nearly 4 kilometers cross-range and 8 kilometers down-range by ignoring oblateness (14:94).

Determining the effects on impact location of the oblate earth involves the solution of a more precise representation of gravitational potential than the simple inverse-square field assumed previously. One such function is

$$\Phi = \frac{\mu}{r} \left(1 - \sum_{n=2}^{\infty} J_n \left(\frac{r_e}{r} \right)^n P_n \sin L \right) \quad (61)$$

where r (burnout altitude) and μ (earth gravitational constant) are as before, r_e is the equatorial radius of the earth, J_n are experimentally derived constants, P_n are "Legendre polynomials", and L is the geocentric latitude (14:19). This equation may be expanded as far as desired and partial derivatives taken with respect to each coordinate axis to determine acceleration effects in each direction. Analysis of oblateness by itself requires only the inclusion of the J_2 term, which corresponds to that effect. The following down-range (δR) and cross-range (δC) equations represent the displacement of the theoretical impact point due to oblateness (14:93):

$$\delta \bar{R} = \frac{-(3/2)J_2 r_e}{Q^2 \cos^3 \phi_{bo} \sin \phi_{bo}} \left[2\left(\frac{1}{3} - A^2\right)(1 - \cos \Psi) + \left(Q \cos^2 \phi_{bo} - \frac{2}{3}\right) \left[(1 - \cos \Psi) + A^2(\cos^2 \Psi + \cos \Psi - 2) - B^2(1 - \cos \Psi)^2 - 2AB \sin \Psi(1 - \cos \Psi) \right] \right] \quad (62)$$

$$\delta C = \frac{-3J_2 r_e}{Q \cos^2 \phi_{bo}} \left(\frac{\sin \Theta \cos L_{bo} \cos L_{re}}{\sin \Psi} \right) (A(1 - \cos \Psi) + B(\Psi - \sin \Psi)) \quad (63)$$

New terms in these equations are the latitudes of the burnout (L_{bo}) and re-entry (L_{re}) points, the equatorial longitude difference between them (Θ), and the constants A and B , which are defined as (14:92)

$$A = \sin L_{bo} \quad (64)$$

$$B = \cos L_{bo} \left(1 - \frac{\cos^2 L_{re} \sin^2 \Theta}{\sin^2 \Psi} \right) \quad (65)$$

The oblateness constant $J_2 = 1.08264 \times 10^{-3}$ (1:424)(14:95). Finally, Ψ is related to L_{bo} , L_{re} , and Θ by (14:87)

$$\cos \Psi = \cos L_{bo} \cos L_{re} \cos \Theta + \sin L_{bo} \sin L_{re} \quad (66)$$

Note that under the non-rotating earth assumption Θ is straightforward in calculation. If rotation is factored in, then Θ is the sum of the longitudinal difference of the burnout and target points and the additional angular amount travelled by the target due to earth rotation.

Actual re-entry point location depends on the nominal latitude and longitude differences of the burnout and re-entry points, which determines the "target value" for free-flight range (Ψ). The particular system design dictates the burnout Q -value and flight-path angle (ϕ_{bo}) necessary to achieve this range. The non-spherical nature of the earth causes displacement in the planned re-entry point, requiring latitude and longitude "corrections" to the planned burnout point to ensure arrival at the desired "re-entry target". The extent of these corrections depends on the particular mission profile, yet should be included to minimize any chance of inducing a bias due to this kind of systematic error.

C.2 Atmospheric Drag During Re-entry

The final portion of a re-entry vehicle's flight is the shortest in duration, yet exposes it to the harshest conditions of heat and deceleration. A re-entry vehicle must arrive at the planned re-entry point and follow the predicted course to accurately arrive at its intended impact point. The vehicle's flight during the re-entry portion of its mission determines where impact actually occurs.

Significant effort in re-entry texts is devoted to examining the interaction between the atmosphere and re-entry vehicles (RVs), which takes the form of deceleration due to atmospheric drag (14)(20). Specific effects are design dependent, but some comments can be made about general effects. Ballistic re-entry vehicles are typically designed with small area/mass ratio and low drag. These characteristics are incorporated to "minimize the effects of trajectory curvature and thus reduce any possible targeting error caused by local winds and atmospheric conditions" (20:222).

If there were no gravity or drag effects, the RV would impact at a point down-range of the re-entry point as given by the equation

$$X = X_{re} + \cot \phi_{re}(H - H_{re}) \quad (67)$$

where X_{re} is the assumed range origin, H_{re} the initial altitude, and H the final altitude (the surface) (20:223). To introduce the perturbing effects first requires the definition of the "drag parameter" K_d , given by

$$K_d = - \left(\frac{A}{m} \right) \frac{C_d H_{re}}{\sin \phi_{re}} \quad (68)$$

where (A/m) is the area/mass ratio and C_d is the drag coefficient determined by the shape of the vehicle (20:220). Since (A/m) and C_d are assumed to be small and H_{re} is fixed, the value of K_d depends mostly upon ϕ_{re} and is minimized as ϕ_{re} approaches the vertical. Wiesel rigorously developed the equation for down-range impact location that accounts for drag effects, but only the result is given below (20:219-223).

$$\begin{aligned}
X = & X_{re} + \cot \phi_{re}(H - H_{re}) \\
& + \frac{\cos \phi_{re}}{v_{re}^2 \sin^2 \phi_{re}} \left[\frac{1}{2} \left(g - \frac{v_{re}^2 \cos^2 \phi_{re}}{R} \right) (H - H_{re})^2 \right. \\
& \left. + K_d g \rho_o H_{re}^2 e^{-(H/H_{re})} \right]
\end{aligned} \tag{69}$$

where g is the gravity acceleration and ρ_o is the "base density of the atmosphere" (20:84). The first two terms of the equation give the previously mentioned "straight line" trajectory, the second line represents the effects of gravity, and the last term gives the effect of atmospheric drag (20:223). Figure 41 shows one plot of this equation for a specific set of starting conditions where the re-entry began at a height of 70 km. For $K_d = 0$, the trajectory is subject only to gravity effects. The chart shows that higher drag results in more pronounced deviation from the theoretical trajectory impact point.

Figure 41. Typical Ballistic Re-Entry Drag Effect (reproduced from (20:224))

C.3 Rotating Earth Effects

Burnout conditions in a non-rotating earth system are set to connect the burnout point with the re-entry point. Adding a rotating earth does not change this basic idea, but the burnout conditions must be modified to take into account the fact that the launch site is "moving" to begin with, and the target point is also moving. Burnout conditions must be designed to "lead" the target to achieve a hit; the planned trajectory does not intersect the target but is designed so that the target point "arrives" by earth rotation simultaneously with the vehicle. Hence, the re-entry "aim point" is co-latitude with the intended target but at some distance east, with this distance equal to the angle through which the earth will rotate during the vehicle's time of free flight (1:309).

C.3.1 Terms and Reference Frames All of the terms previously used remain in effect, but this particular problem will require an additional term and a new coordinate reference frame. The *topcentric-horizon* coordinate system (TH) is used to make measurements relative to a given location on or near the earth's surface. The origin of the system is at that location, the positive- x axis points toward the south pole, the positive- y axis points eastward, and the positive- z axis is orthogonal to these following a right-hand rule. For example, if the location is a launch pad on the earth's surface, positive- z would point "up" at the sky. The system is represented in terms of the unit vectors $\vec{s}, \vec{e}, \vec{z}$, corresponding to the x - y - z axis directions, respectively (1:84). Additionally, the *azimuth angle* is the term which defines the direction of launch and is measured from the $-\vec{s}$ (a.k.a. "north") axis to the velocity vector.

C.3.2 Burnout Conditions The parameters of burnout are r_{bo} , v_{bo} , and ϕ_{bo} , but these must now be expressed in the TH system, which takes into account the earth's rotational velocity. As shown in Figure 42, the velocity vector can be broken into its TH components using ϕ and β , which represents the azimuth angle. An additional term must be added to the eastward component of the velocity due to the eastward rotation of the earth. The components of burnout velocity may be written mathematically (1) as

$$v_s = -v_{TH} \cos \phi_{TH} \cos \beta \quad (70)$$

$$v_e = v_{TH} \cos \phi_{TH} \sin \beta + v_o \quad (71)$$

$$v_z = v_{TH} \sin \phi_{TH} \quad (72)$$

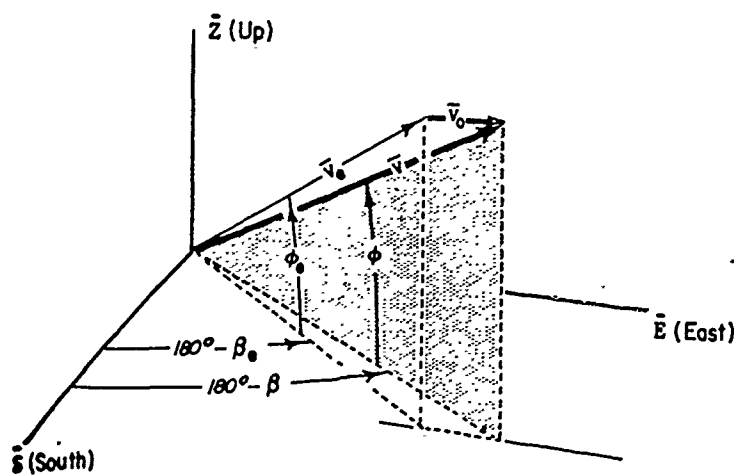


Figure 42. Velocity Components in the TH System (reproduced from (1:309))

where the subscript *TH* represents the burnout conditions relative to the TH reference frame, and which may have been determined by measurement from the launch site. The value for v_0 is launch site latitude dependent, and may be determined from the equation

$$v_0 = 1524 \cos(L_l), \quad (73)$$

expressed in *ft/sec*, and with L_l the launch point latitude (1:307). Using vector mathematics, "real" values of the burnout parameters may be determined corresponding to the inertial reference frame. As shown in (1:308),

$$v_{bo} = \sqrt{v_s^2 + v_e^2 + v_z^2} \quad (74)$$

$$\phi_{bo} = \sin^{-1}\left(\frac{v_z}{v_{bo}}\right) \quad (75)$$

and additionally,

$$\beta = \tan^{-1}\left(\frac{-v_e}{v_s}\right) \quad (76)$$

Since the trajectory is primarily determined by burnout, earth rotation affects the trajectory. For a particular range, the earth contributes to the total required velocity if the launch is in the direction of the earth's rotation. With a fixed payload weight, the vehicle could in theory deliver it further eastward than westward. Given a range

that is obtainable in either direction, a heavier payload could also be launched by taking advantage of the earth's rotational velocity.

A Pegasus-based vehicle leads to some additional considerations. There would be an additional velocity term in each component direction owing to the movement of the carrier aircraft. Also, since it is not restricted to a fixed launch site, the vehicle could conceivably guarantee advantageous use of earth rotational velocity by having the carrier fly to the appropriate launch point. Figure 43 shows the added eastward velocity imparted by earth rotation, and the velocity lost by westward launch.

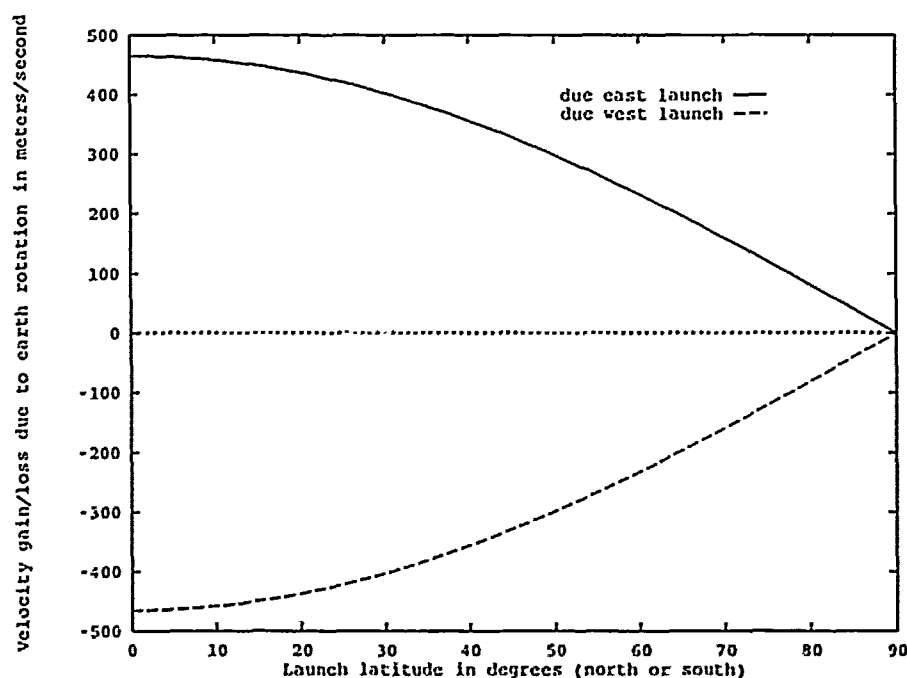


Figure 43. Velocity Effects of Earth Rotation

C.3.3 Re-entry Location Determination The distance that the earth rotates during vehicle flight must be determined before a trajectory can be assigned. In Chapter 3, Θ was defined as the difference in longitude between the burnout and re-entry points. In the rotating earth case, the value of Θ is that of the non-rotating case, determined by the ellipse geometry, *plus* an additional amount determined by the vehicle flight time and earth rotation rate. From Eq (65), the range angle is related to the latitudes of burnout and re-entry and the longitude difference. Θ is

defined for the rotating earth case by the equation

$$\Theta = \Theta_o + \omega_e \Delta t \quad (77)$$

where Θ_o is the longitude difference between launch re-entry points and Δt is the time of flight from burnout to re-entry.

Azimuth may be incorporated into the problem by using the spherical law of cosines:

$$\sin L_{re} = \sin L_{bo} \cos \Psi + \cos L_{bo} \sin \Psi \cos \beta \quad (78)$$

Once the velocity components and burnout altitude have been determined, corresponding values for Q and ϕ_{bo} can be determined. Using Eq (24), Ψ can be determined, and therefore Eq (68) can be solved for the re-entry latitude point.

Determination of re-entry point longitude depends upon time of flight, which can be determined by solving Eq (57) for the particular parameters in question. Once this has been determined, Eq (65) may be used to determine re-entry longitude location.

Bibliography

1. Bate, Roger R. et. al. *Fundamentals of Astrodynamics*. New York: Dover Publications, Inc., 1971.
2. Elder, Capt Richard L. *An Examination of Circular Error Probable Approximation Techniques*. MS Thesis AFIT/GST/ENS/86M-6. School of Engineering, Air Force Institute of Technology (AU), Wright-Patterson AFB, OH, May 1986.
3. Flemings, Maj Garrison H. Personal interviews. AFIT/GST 92-M. Wright-Patterson AFB OH, October-November 1991.
4. Jasani, Bhupendra ed. *Space Weapons-The Arms Control Dilemma*. Philadelphia: Taylor & Francis, Inc., 1984.
5. Lindberg, Robert E. "The Pegasus Air-Launched Space Booster," *26th Space Congress Proceedings*. 5-31-5-38. Cocoa Beach, Florida: Canaveral Council of Technical Studies, 1989.
6. Meyer, Scott K. "Top-Down Analysis," *The Executive Analyst*, 1.1:1-2 (May 1986).
7. Meyer, Scott K. "Top-Down Modelling," *The Executive Analyst*, 1.2:1-6 (March 1987).
8. Office of the Secretary of the Air Force. *The Air Force and US National Policy: Global Reach-Global Power*. White Paper. Washington: US Government Printing Office, June 1990.
9. Office of the Secretary of Defense. *Department of Defense Space Policy*. Memorandum for Correspondents. 10 March 1987.
10. Office of the White House Press Secretary. *US National Space Policy*. Fact Sheet. 6 November 1989.
11. Orbital Sciences Corporation and Hercules Aerospace Company. *First Pegasus Launched Successfully; Rocket Places Satellites in Orbit*. News Release. 5 April 1990.
12. Orbital Sciences Corporation and Hercules Aerospace Company. "Pegasus Flight 001, 5 April 1990 Quick Look Data Report". Briefing for AFSPACE-COM Commander. Peterson AFB CO, April 1990.
13. *Pegasus Payload User's Guide Release 2.00*. Orbital Sciences Corporation, Fairfax, Virginia, 1 May 1991.
14. Regan, Frank J. *Re-Entry Vehicle Dynamics*. AIAA Education Series. New York: American Institute of Aeronautics and Astronautics, Inc., 1984.

15. Reiersen, James D. et. al. *Techniques for Bomber Range-Payload and Refueling Calculations*. Strategic Branch Note SBN 70-2. Analytic Services, Inc., April 1970 (AD 510501).
16. Space Systems Division/XR, Air Force Systems Command. "Global Precision Response Capability: An Innovative Tactical Weapon System." Briefing to AF-SPACE/COM. Peterson AFB, Colorado, December 1990.
17. Stares, Paul B. *The Militarization of Space*. Cornell Studies in Security Affairs. Ithaca, New York: Cornell University Press, 1985.
18. Sutton, George P. *Rocket Propulsion Elements: An Introduction to the Engineering of Rockets*. New York: John Wiley & Sons, Inc., 1986.
19. Venttsel, Ye. S. Introduction to Operations Research. Translation from the Russian textbook "Vvedeniye v issledovaniye operatsiy". Moscow: "Soviet Radio" Publishing House. 1964.
20. Wiesel, William E. *Spaceflight Dynamics*. McGraw-Hill Series in Aeronautical and Aerospace Engineering. New York: McGraw-Hill, Inc. 1984.
21. Wolf, Capt James R. "Toward Operational-Level Doctrine for Space: A Progress Report," *Airpower Journal*, 5.2: 28-40 (Summer 1991).